Title
Engineering Biomaterials and Biomolecules for Vascular Regeneration

Author
Huang, Fang

Publication Date
2016

Peer reviewed|Thesis/dissertation

Engineering Biomaterials and Biomolecules for Vascular Regeneration

by

Fang Huang

A dissertation submitted in partial satisfaction of the

requirements for the degree of

Joint Doctor of Philosophy
with the University of California, San Francisco

in

Bioengineering

in the

Graduate Division

of the

University of California, Berkeley

Committee in charge:

Professor Song Li, Chair
Professor Randall Lee
Professor Liwei Lin

Fall 2016

Abstract

Engineering Biomaterials and Biomolecules for Vascular Regeneration

by

Fang Huang

Joint Doctor of Philosophy
with the University of California, San Francisco

in Bioengineering

University of California, Berkeley

Professor Song Li, Chair

Tissue engineering and regenerative medicine is a multidisciplinary field that combines the knowledge and technologies of biology, materials, chemistry and medicine among others. Within the realm of tissue repair and regeneration, vascular reconstruction, in particular, is influenced by both biophysical and biochemical cues and it is critical to fully understand how these cues interact with the physiological microenvironment. In this dissertation, we demonstrated how host vascular regenerative potential can be harnessed by optimizing vascular grafts from both the biomaterial and biochemical perspectives. We utilized and optimized electrospinning technology to create microfibrous vascular grafts. We showed that incorporating a fast degrading polymer into the vascular grafts effectively enhances cell infiltration without majorly compromising its mechanical and structural properties. Our *in vivo* data suggests that although the optimized vascular graft was able to induce the initiation of vascular regeneration, the process was accelerated and enhanced with the help of biochemical cues presented in the form of stromal cell-derived factor-1α (SDF-1α). In the presence of chemokine SDF-1α, the vascular grafts demonstrated better wall remodeling and long-term patency. This observation again highlights the significance of both biomaterial and biochemical effects. While the vascular grafts in our studies might recruit inflammatory cells, calcification which is a destructive complication typically associated with inflammatory response was not observed. The final part of this dissertation details our efforts in using protein engineering to broaden the biological application of SDF-1α by introducing a free cysteine residue on its *C*-terminus. We showed that the cysteine-modified SDF-1α exhibits a bioactivity different from its unmodified counterpart, the underlying mechanism of which needs to be elucidated in future studies. Taken together, this work is expected to provide insights into optimization of vascular graft platforms for broad therapeutic applications.

Dedication

This dissertation is dedicated to my parents,
Aiguang Huang and Xiangping Zhao,
for their never-ending support, inspiration, encouragement,
and unconditional love.

Acknowledgments

I would, first and foremost, like to thank my family, especially my inspiring parents for all of their support, encouragement, and unconditional love throughout these years. Without them, none of my accomplishments would be possible. I would like to thank my PhD advisor, Dr. Song Li, for providing me the opportunity to embark on the journey of graduate school and conduct graduate research under his guidance and mentorship. I would also like to thank my project mentor and friend, Dr. Shyam Patel, as he truly looked after me and provided me many wise pieces of advice on research and career, as well as moral support over the stressful period. I am grateful to meet and become friends with many brilliant Li Lab members. Together with Tiffany Dai and Weixi Zhong, we shared many laughter and tears, as well as a lot of late nights in the lab. Danny Wen-Chin Huang, Sze Yue Wong, and Helen Ching-Wen Huang have given me much personal and professional help, and I truly appreciate their friendship. I would like to express appreciation to my colleagues who has contributed to the work of this dissertation: Drs. Xuefeng Qiu, Dong Wang, as well as Angela Yu-Fang Hsieh, and Kang Xu. I would also like to show a special gratitude to Dr. Zhenyu Tang, who is a past Li Lab member and provided tremendous help preparing me for graduate school. My appreciations also go to all the current and past Li Lab members for a valuable exchange of knowledge and experiences. Specifically, Julia Chu, Jaren Sia, Jennifer Soto, Doug Kelkhoff, Elaine Su, Julia Chang, Benjamin Li-Ping Lee, Timothy Downing, An-Chi Tsou, and Aijun Wang. I would like to thank all the members who took the time to serve on my dissertation committee (Drs. Song Li, Randall Lee, and Liwei Lin) and qualifying exam committee (Drs. Gerard Marriott, Xiaohua Gong, Bo Huang, and Kyriakos Komvopoulos) for providing thoughtful feedback toward my research. I would also like to acknowledge Drs. Hayley Lam and Amy Herr for making my GSI experience more enjoyable. I am thankful for the funding sources including University of California, Berkeley, and Anselmo Macchi Fellowship for helping to support me during my graduate career. Lastly, I would like to extend my gratitude and acknowledge a number of close friends: Kun Fang, Fan Wu, Karen Liang, Tony Dear, Yi-Pei Li, Reta Zeng, Siwen Deng, and Wincy Tse. I genuinely appreciate their company over the years, and their friendship will always be cherished.

Table of Contents

List of Figures

Chapter 2

Chapter 3

Chapter 4

List of Tables

Chapter 1: Introduction

1.1 Introduction

Tissue engineering and regenerative medicine utilize cells, biomaterials, or a combination of both with applicable biochemical stimuli to repair or replace trauma- or disease-damaged native tissues. Effective tissue engineering and regenerative medicine strategies for treating cardiovascular diseases require sufficient therapeutic revascularization. Many cardiovascular diseases such as cardiac ischemia and peripheral vascular disease are caused by loss of vascular supply, which prevents adequate transportation of oxygen and necessary nutrients/waste exchange, thus leading to cell death and eventual organ failure. Regenerative approaches to treating cardiovascular diseases commonly involve reconstructing vascular bridges for both oxygen and nutrient exchange, and propagation of indispensable paracrine signals. However, vascular regeneration remains challenging due to insufficient and slow recruitment and generation of endothelial cells (1). Although numerous studies have been done to improve vascular regeneration, each approach has its pitfalls and limitations. Therefore, advancement in the technology for vascular regeneration remains a field of vital study.

Tissue repair and regeneration are influenced by both biomaterials and biochemical stimuli. In particular, vascular regeneration frequently relies on the use of biodegradable and biocompatible scaffolds with optional cell seeding, vascular growth factors, and anticoagulants. To fully understand the roles played by these cues in vascular regeneration, more investigation is critical. In this dissertation, we explored the effect of a cell-free biodegradable vascular graft and chemokine stimuli on vascular regeneration. This work provides insights and the groundwork for future studies to develop and optimize a platform for vascular regeneration which can contribute to therapeutic applications.

1.2 Dissertation Outline

In **Chapter 2**, we investigated how modulating electrospinning parameters influences fiber spacing of vascular grafts as it may directly affect the degree and extent of cell infiltration into the scaffolds. In addition, in an effort to improve cell infiltration of our established system, we introduced a fast-degrading polymer in addition to our initial polymer and fabricated multiple vascular grafts with various designs. We subsequently performed a primary screening based on their post-electrospinning morphology and structural integrity, and a secondary screening based on the degree of *in vivo* cell infiltration. We explored the effect of a fast-degrading polymer on cell infiltration and showed a noticeable improvement. Cell infiltration of the vascular grafts is critical for vascular remodeling and regeneration. This information is important for vascular graft fabrication as it allows us to achieve better cell infiltration without severely compromising its mechanical properties.

In **Chapter 3**, we explored the *in vivo* performance of the vascular graft screened in Chapter 2. We demonstrated that the designed vascular graft was able to recruit endothelial cells. In addition, we explored the effect of stromal cell-derived factor-1α (SDF-1α), which is a powerful chemokine that recruits endothelial and smooth muscle progenitor cells, in combination with a designed vascular graft on vascular remodeling; the presence of the chemokine led to better remodeling and long-term patency. Findings from this chapter contribute to our understanding of the effect of biomaterials and biochemical cues on vascular regeneration, in particular, endothelialization and remodeling.

In **Chapter 4**, we shifted our focus from biomaterials to biochemical cues. To broaden the biological applications of the chemokine SDF-1α used in Chapter 3, we engineered a cysteine modified SDF-1α that is readily used for subsequent chemical conjugations. In this chapter, we described the protocol to express, isolate, refold, and purify the cysteine modified SDF-1α. Our investigation of its *in vitro* chemotactic activity showed it has a significantly different activity compared to its unmodified counterpart. These findings allow future studies to build upon our modification and design more potent medicine for therapeutic applications, such as treating tissue ischemia.

Chapter 2: Fast-degrading Polymer Enhances Cell Infiltration into Electrospun Vascular Grafts

2.1 Introduction

2.1.1 Tissue Engineered Vascular Graft

Tissue engineering and regenerative medicine is a fast-growing field centered on creating equivalents to native body tissue for replacement of trauma- or disease-damaged tissue (2-5). In particular, there is a great need for the replacement of obstructed blood vessels. According to a 2012 statistics report from the American Heart Association, cardiovascular disease accounts for more than one-third of all deaths and is the leading cause of death in the United States (6, 7). As arterial replacement is the most common treatment for vascular diseases, the field of vascular tissue engineering has undergone rapid development in the past two decades (8).

Every year in the United States, over 500,000 vascular grafts are used in bypass procedures for coronary arteries and peripheral arteries. Most of the vascular grafts used are autologous grafts (8). An autologous graft is a graft, venous or arterial, harvested from another site of the patient's body. It has the advantages of being native and biocompatible to the patient, free of immune rejection, and having optimal biological, structural, and mechanical properties. However, the use of autologous graft is limited by its availability: one-third of patients with the peripheral arterial disease do not have suitable autologous grafts (9-11). Moreover, harvesting autologous grafts requires additional surgeries and may potentially lead to donor site morbidity.

When availability limits the use of autologous grafts, polymer-based synthetic vascular grafts are used as an alternative. Commercially available polymer-based synthetic vascular grafts are usually made of expanded-polytetrafluoroethylene (ePTFE), Dacron or polyurethane (12, 13). Although these polymers are biological inert, their lack of anti-thrombotic properties restricts their usage as small-diameter grafts, which have a higher frequency of developing thrombosis and occlusion.

Given the advantages and disadvantages of autologous and synthetic grafts, many researchers have focused on developing readily available small-diameter (<6mm) tissue-engineered vascular grafts that possess the same biological, biochemical, and mechanical properties as native vessels. To achieve the desired functional vascular grafts, some strategies utilize decellularized allogeneic or xenogeneic vessels (14-16) and electrospun vascular grafts using synthetic and/or natural polymers in combination with various cell types and/or biochemical molecules (17, 18). Summary of *in vivo*, *in vitro*, and *in situ* approaches to generate vascular grafts is illustrated in Figure 2.1.

2.1.2 Electrospinning

Electrospinning is a convenient method for creating scaffolds that mimic the physiological microstructure of native tissue (19). The general process of

electrospinning involves dissolving polymers in a highly volatile solvent such as chloroform or HFIP (hexafluoro-2-propanol). The polymer can either be synthetic (e.g., PLLA, PEG, or PEO) or natural (e.g., fibrin, collagen, or fibronectin). The polymer solution is ejected through a syringe needle using a syringe pump. Ejected solution is exposed to a high electrical field, which causes the solvent to evaporate instantly. The solute then "whips" back and forth to produce a continuous fiber. The fiber travels across a certain distance and is collected onto a target (20, 21). The use of electrospinning has the following advantages: the fibers formed have diameters similar to those seen in collagen fibrils and provide a cellular architecture similar to that found in native biological tissue, which allows integration of the grafts with surrounding cells and tissues (21, 22); various properties of the scaffold such as fiber diameter, mechanical strength, or porosity can be precisely tuned by modulating electrospinning parameters such as voltage, needle distance, polymer concentration, and polymer solution flow rate (23-25).

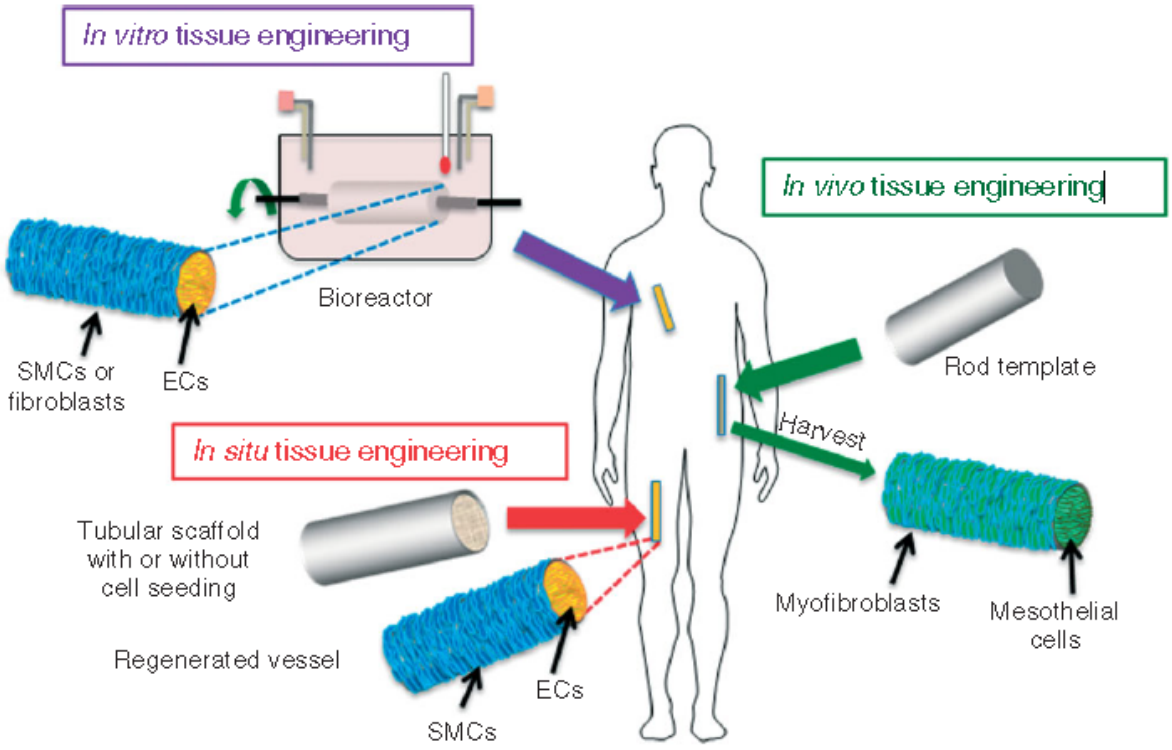

Figure 2.1 Schematic illustration of *in vitro*, *in vivo*, and *in situ* approaches to generate vascular grafts (8).

2.1.3 Polymer

A polymer is a long macromolecule composed of many repeating building blocks. These repeating units are called monomers. Depending on its origin, a polymer can be natural or synthetic. Natural polymers such as protein, starch, cellulose, and natural rubber are obtained from natural sources. Synthetic polymers such as polyethylene, polystyrene, and polyurethanes can be synthesized chemically in the laboratories (26,

27). The chemical and physical properties of a polymer are greatly influenced by its synthesis condition, such as the polymerization mechanism, type, and amount of input monomer, initiator, and catalyst (27). This characteristic allows us to fine-tune the synthesis condition to produce polymers that fit specific needs.

Poly(L-lactide-co-ε-caprolactone)

Synthetic biodegradable polymers such as homopolymer PLA (polylactide), PCL (poly(ε-caprolactone)) and their copolymer PLCL (Poly(L-lactide-co-ε-caprolactone)) have been widely employed clinically (28). They have been utilized for various medical applications, such as sutures, orthopedic, drug delivery systems, and scaffolds for tissue engineering. Copolymer PLCL, which has a physically cross-linked structure, is formed from two different monomers: L-lactide and ε-caprolactone. It exhibits a rubber-like elasticity owing to its soft matrix of mainly ε-caprolactone moieties and hard domains composed of additional L-lactide units (29). Due to the different roles played by the two types of monomer, mechanical properties such as elasticity and degradation rate of the copolymer PLCL are largely affected by the monomer content (29, 30). PLCL is biodegradable and degrades *in vivo* primarily by hydrolysis into non-toxic end products (29). In addition, PLCL is compatible with electrospinning and has been extensively used to produce scaffolds for vascular tissue engineering (31).

Polydioxanone

Polydioxanone (PDO) is a colorless, biocompatible, and biodegradable polymer that is initially developed for use as wound closure sutures (32). As a suture, it exhibits high flexibility. When compared to other suture materials such as Vicryl or Dexon, PDO demonstrates higher strength retention, slower absorption rates, and lower inflammatory response rates (33). When PDO is used as a typical monofilament suture, it loses 50% of its initial breaking strength after three weeks and is completely absorbed within six months (an advantageous time scale for slower wound healing) (33, 34). PDO is compatible with electrospinning to produce fibers. Electrospun fibers of PDO possess diameters ranging from hundreds of nano- to micrometers. Moreover, electrospun PDO scaffolds have mechanical properties comparable to collagen and elastin, two major structural components of blood vessels (35). Overall, the combination of biocompatibility, flexibility and degradation rate of PDO makes PDO a potential candidate for tissue engineering applications including vascular grafts.

2.2 Materials and Methods

2.2.1 Fabrication of Vascular Grafts

Electrospinning was performed to fabricate vascular grafts. The electrospinner set-up (Figure 2.2A) consists of a programmable syringe pump that is used to dispense polymer solution from a 25 mL syringe, silicone tubing used to connect syringe and a stainless steel 25G dispensing needle, a stainless steel mandrel that rotates at 16 rpm to collect electrospun fiber, and a spinneret that traverses in parallel direction with rotating collector to ensure resulting vascular grafts have uniform thickness in its longitudinal direction. Two high-voltage generators were used to apply negative voltage of 3 kV to the mandrel and a positive voltage of 11 kV to the spinneret. The electrospinning process was allowed to continue until the desired wall thickness was achieved based on measurements obtained with a thickness gauge. Three different formulations of polymer solution were used in this study:

- The PLCL (70 wt% L-lactide and 30 wt% ε-caprolactone) solution was made by dissolving 15% PLCL (w/v), 1% PPG (v/v) in Tris-HFIP which contains 0.05% w/v Tris-HCl.
- The PDO solution was made by dissolving 20% PDO (w/v) in Tris-HFIP.
- The PLCL/PDO blend solution was made by mixing aforementioned PLCL and PDO solution at 1:1 ratio by volume.

All polymer solutions were secured to an orbital rotator and allowed to dissolve overnight in a fume hood.

2.2.2 Manufacturing PLCL Vascular Grafts with Various Fiber Spacing

The PLCL grafts were fabricated as described in Section 2.2.1. To modulate fiber spacing of the electrospun grafts, while the other parameters (voltage, polymer concentration, needle gauge, and mandrel rotating speed, etc.) were kept consistent, two parameters were independently manipulated: (1) the flow rate (FR) at which polymer solution was dispensed from the syringe; and (2) the distance between needle and rotating mandrel, i.e., the mandrel-needle distance (MND).

Three different FRs at 1, 3, and 5 mL per hour were tested. At each FR, the grafts were electrospun at two different MND: 9, and 11 cm, giving a total of six combinations. A scanning electron microscope (SEM, Hitachi TM-1000) was used to examine and image the fiber spacing on the luminal surface for each experimental group.

2.2.3 Structuring Single- and Multi-Layered Vascular Grafts with PLCL and PDO

All electrospinning parameters were kept consistent as described in Section 2.2.1 with FR at 3 mL/h and MND at 11cm. Using the three different formulations of polymer

solution (15% PLCL, 20% PDO, and PLCL/PDO blend), four single-layered and three multi-layered vascular grafts were fabricated.

To produce single-layered vascular grafts, the three aforementioned polymer solutions were independently used to spin PLCL, PDO, and PLCL/PDO blend grafts. The fourth single-layered vascular graft was manufactured by co-electrospinning a 15% PLCL and a 20% PDO solution as follows: two syringes containing 15% PLCL and 20% PDO solution were attached to the same syringe pump so that their rates at dispensing polymer solution were identical. Two silicone tubing were separately connected to the two syringes. The polymer solutions were eluted from two different needles that were both secured to the same spinneret. The resulting electrospun fibers were collected onto the same mandrel. The aforementioned four single-layered vascular grafts will be referred to as PLCL, PDO, PLCL/PDO blend, and PLCL/PDO co-spun, respectively.

To produce multi-layered vascular grafts, 15% PLCL and 20% PDO polymer solutions were used. Only one polymer solution was allowed to spin at any one time. One solution was allowed to electrospin for a certain amount of time until the graft wall reached the desired thickness; the solution was subsequently switched to the other formulation immediately, and spinning was allowed to continue until the final thickness reached approximately 200 to 250μm. The three structures manufactured in this study are as follows:

- PLCL as luminal layer (~50μm) and PDO as exterior layer.
- PDO as luminal layer and PLCL as exterior layer (~50μm)
- PLCL as middle layer (~50μm) and PDO as both luminal and exterior layer.

The aforementioned three multi-layered vascular grafts will be referred to as PLCL-L, PLCL-E, and PLCL-M, respectively.

2.2.4 *In Vivo* Subcutaneous Implantation and Explantation

The animal protocol was developed and approved before surgery. All procedures were approved by the Institutional Review Board Service and the Institutional Animal Care and Use Committee at the University of California, Berkeley. 2-month-old male Sprague-Dawley (SD) rats (approximately 260g) were purchased from the Charles River animal facility. The rats were anesthetized with 2.0% isoflurane in 70% nitrous oxide and 30% oxygen. Abdominal skin was dissected; single-layered vascular grafts (PLCL electrospun at different MND, PDO, PLCL/PDO blend, and PLCL/PDO co-spun) were placed in between fascia and muscle without being sutured to surrounding tissue. The wound was sutured with a 4-0 needle. After 2 or 4 weeks *in vivo*, the animals were euthanized, and the vascular grafts were explanted.

2.2.5 Histological Analysis

The grafts were explanted and fixed with 4% paraformaldehyde (PFA) for 2 hours and dehydrated in 30% sucrose overnight at 4^{o}C. The dehydrated grafts were frozen in

an optimal cutting temperature (OCT) compound (Tissue-Tek), and sectioned into 10μm-thick slices using a cryostat.

Hematoxylin and Eosin (H&E) Stain

Hematoxylin and Eosin (H&E) staining was performed to determine the degree of cell penetration into the grafts. Slides were fixed again with 4% PFA for 10 minutes. Fixed slides were washed with water for 5 minutes and followed by hematoxylin staining for 15 minutes. Slides were quickly rinsed with water and stained with eosin for 1 minute. Stained slides were dehydrated for 2 minutes each with increasing concentrations of ethanol (70%, 85%, and 100% ethanol) and followed by Xylene for 5 minutes to clear residual ethanol. The finished slides were air-dried and mounted with xylene-based Permount medium.

2.3 Results

2.3.1 Fabrication of Microfibrous Vascular Grafts

As shown in Figure 2.2A, an electrospinning technique was used to fabricate microfibrous tubular grafts. Representative images obtained by SEM showed that the fibers produced by electrospinning have diameters varying from the nano- to micro-scale, and the electrospun grafts have a porous structure (Figure 2.2B). Electrospun tubular grafts comprise both a luminal surface and an exterior surface. Fibers on the luminal surface have smaller diameters and fiber spacing in comparison to the exterior surface, resulting in a “denser” luminal surface and a “looser” exterior surface. The porous surfaces were observed along the longitudinal direction as well as the radial direction as shown in the SEM image of vascular graft cross-section (Figure 2.2B). When it is more exterior along the radial direction, the graft becomes more porous. This observed pattern is consistent with the previous observation that the luminal graft is “denser” than the exterior graft.

2.3.2 Effects of Fiber Spacing of PLCL Grafts on *In Vivo* Cell Infiltration

To determine the effect of electrospinning parameters on the fiber spacing of electrospun vascular grafts, the PLCL solution was electrospun under different conditions. Two electrospinning parameters, the FR and the MND were modulated while the rest of the electrospinning parameters were kept consistent. The polymer solution was electrospun at a FR of 1, 3, or 5 mL per hour, while the MND was kept at either 9 or 11 cm. The SEM images of the luminal surfaces of the vascular grafts showed that varying the FR of the polymer solution does not noticeably change the fiber diameter or spacing between fibers (Figure 2.3). When the MND was kept consistent, changing the polymer solution FR from 1 to 3 mL per hour, or from 3 to 5 mL per hour did not affect the morphology of vascular graft. The luminal surfaces of all grafts with a fixed MND were approximately equally “dense.” In contrast, MND does affect the fiber diameter and spacing between fibers. While the other parameters were fixed, when the MND was reduced from 11cm to 9cm, the electrospun fibers had a distinctly bigger diameter. In addition, the grafts had a bigger pore size and hence a “looser” structure. As demonstrated, it is possible to produce more porous grafts by reducing the MND; however, there is a limitation on this approach. When the MND was reduced to below 9cm, instead of being electrospun as a single fiber, the PLCL polymer solution was electrosprayed onto the rotating mandrel and created grafts with undesirable properties (data not shown). Therefore, under the reported electrospinning condition with our electrospinner setup, the shortest distance between mandrel and needle to allow PLCL electrospinning is 9cm.

To determine whether the pore size difference achieved by altering the MND is sufficient to influence cell infiltration *in vivo*, PLCL vascular grafts electrospun at a MND of 9cm and 11cm were subcutaneously implanted into 2-month-old male SD rats. 2 weeks following implantation, the grafts were explanted, and H&E staining was performed to visualize cell infiltration. As shown in Figure 2.4, at 2 weeks, cells have

infiltrated into the grafts. For both groups, there were more cells at the outer rim of the grafts than on the inside, as expected. However, it is surprising to see that the electrospun MND-9cm grafts, which have noticeably larger pore size, had marginally more cells infiltrated into the grafts compared to electrospun MND-11cm grafts. Unfortunately, the greatest extent of cell infiltration obtained with PLCL vascular grafts is still below satisfactory, suggesting a different approach is needed to enhance cell infiltration.

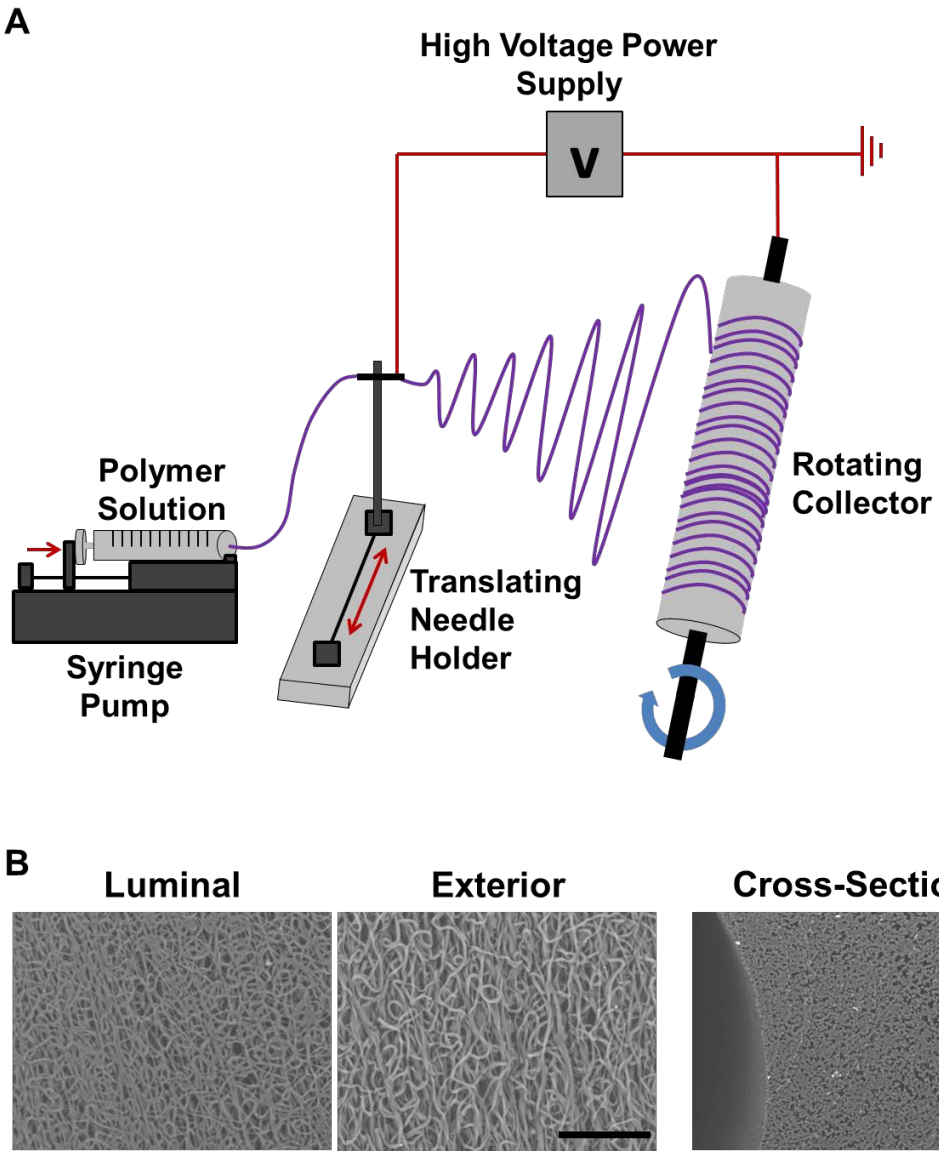

Figure 2.2 Electrospinning and microstructure of electrospun vascular grafts. (A) Set-up and process of electrospinning. (B) Representative structure of luminal (left), exterior (middle) and cross-section (right) surface of an electrospun vascular graft. Scale Bar = 50μm.

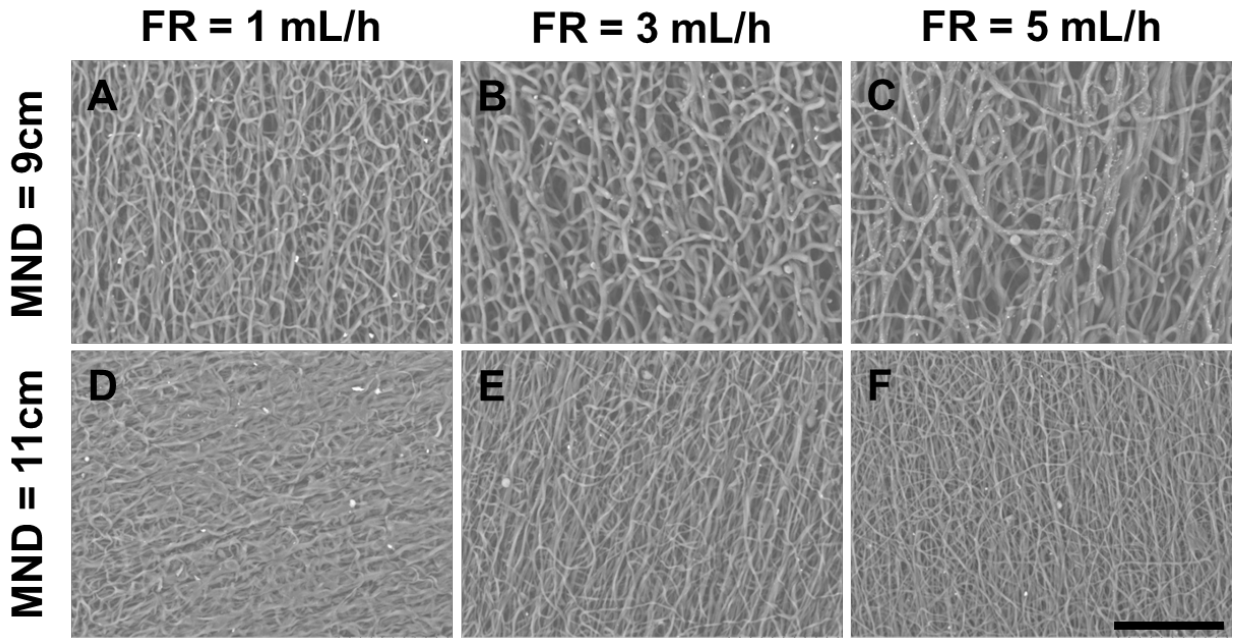

Figure 2.3 Characterization of electrospun microfibrous PLCL vascular grafts. The luminal surface of PLCL vascular grafts electrospun at varying polymer solution FRs at a MND of (A-C) 9 cm and (D-F) 11 cm. Scale Bar = 50μm.

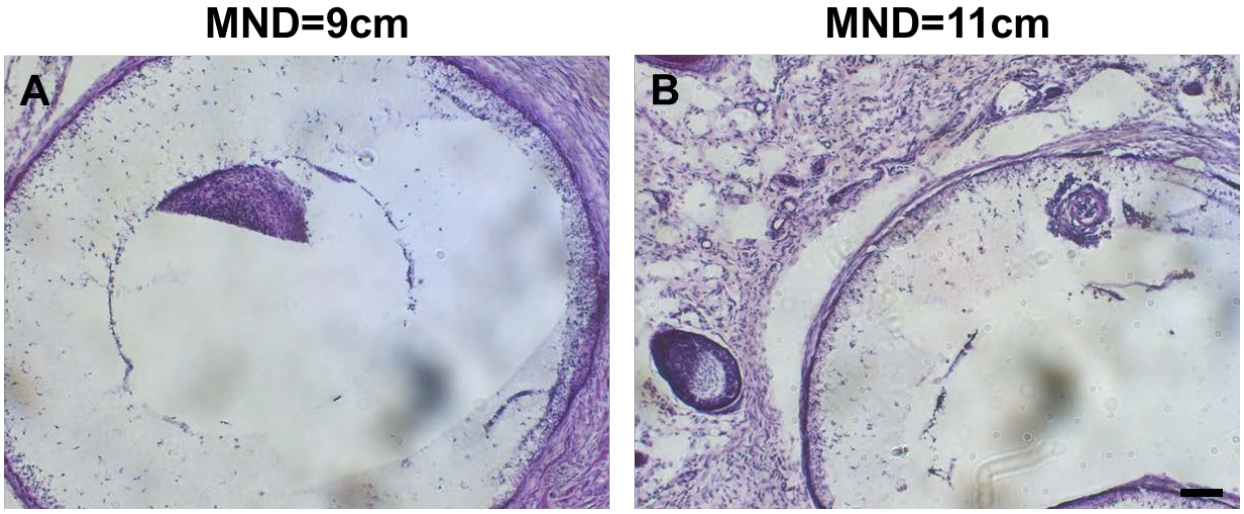

Figure 2.4 *In vivo* cell infiltration of the microfibrous vascular grafts. H&E staining of PLCL vascular grafts electrospun at a MND of (A) 9cm and (B) 11cm 2 weeks after subcutaneous implantation. Scale Bar = 100μm.

2.3.3 Structuring of Single- and Multi-layered Vascular Grafts with PLCL and PDO

PDO is a fast degrading polymer. Our preliminary data (not shown) has demonstrated that electrospun PDO sheet loses its mechanical strength drastically *in vitro* after a month, suggesting it could potentially serve as the sole graft material or as an additive to PLCL vascular graft to promote cell infiltration. We optimized electrospinning parameters for PDO grafts prior to further studies. Although PDO has a similar chemical structure compared to PLCL, their properties differ slightly. As a result, PDO does not electrospin as satisfactorily under the conditions optimized for PLCL.

Initial attempts to electrospin 12% PDO in Tris-HFIP (w/v) resulted in grafts with rough exterior surfaces (Figure 2.5A-B). Moreover, the PDO lacks the strong intermolecular adhesion of PLCL, resulting in severe delamination (Figure 2.5C). The issues of rough surface and delamination were not alleviated by adjusting the electrospinning parameters (i.e., voltage, MND, and FR, etc.). To address these issues, we increased the concentration of polymer solution. We electrospun PDO grafts with a gradient of polymer concentration, ranging from 12% to 20%. The results showed that higher concentrations of PDO resulted in smoother graft surfaces. The 20% PDO grafts have an exterior surface approximately as smooth as the optimized PLCL grafts, as shown in Figure 2.5D-E. The SEM images of the cross-section of the 20% PDO grafts (Figure 2.5F) showed that its structural integrity is superior to 12% PDO grafts, yet still not as good as 15% PLCL grafts. However, its weaker structural integrity leads to a more porous structure, which is potentially beneficial for cell infiltration.

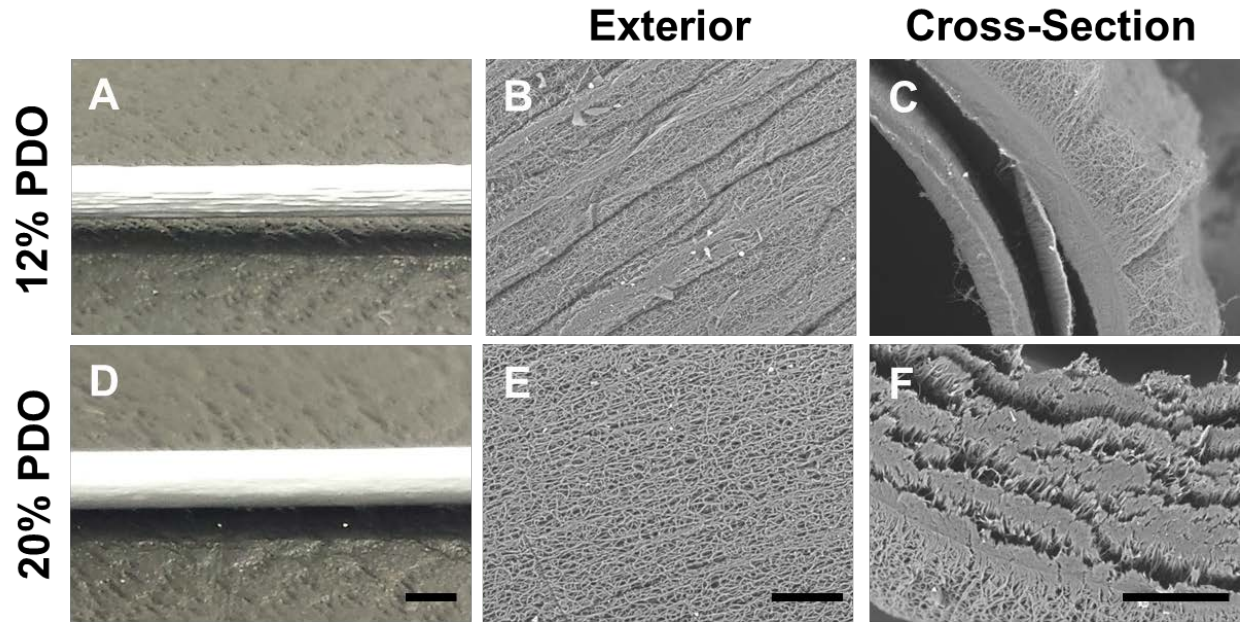

Figure 2.5 Characterization of electrospun microfibrous PDO vascular grafts. Gross structure (A, D, scale bar = 1mm) and SEM images of microstructure of exterior (B, E, scale bar = 100μm) and cross-section (C, F, scale bar = 100μm) surface of PDO vascular grafts electrospun at 12 and 20 wt%.

In addition to 15% PLCL and 20% PDO grafts, two other single-layered vascular grafts were fabricated: 15% PLCL and 20% PDO solution was thoroughly mixed with a 1:1 ratio and the mixed solution was electrospun to make PLCL/PDO blend grafts. The PLCL/PDO co-spun grafts were fabricated by co-electrospinning 15% PLCL solution and 20% PDO solution using two spinnerets simultaneously. The SEM images of luminal surfaces of the vascular grafts showed that 20% PDO, PLCL/PDO blend, and PLCL/PDO co-spun grafts have comparable morphology, and they all have larger fiber spacing and thicker fibers compared to 15% PLCL grafts (Figure 2.6A). The SEM images of cross-section surfaces of the vascular grafts showed that PLCL/PDO blend grafts have similarities to both 15% PLCL and 20% PDO grafts. The blend grafts have organized morphology and structural integrity similar to PLCL grafts; yet, they are similar to 20% PDO grafts and possess a more porous structure than PLCL. Compared to the PLCL/PDO blend grafts, which essentially have a balanced structure of 15% PLCL and 20% PDO grafts, the PLCL/PDO co-spun grafts have a more interesting and surprising architecture. Theoretically, PLCL/PDO co-spun grafts ought to show a single-layered structure as the two spinnerets were run simultaneously. Yet, SEM images showed it carries a non-delaminated “stacked” structure, with alternating layers of PLCL’s and PDO’s look-alikes. However, any theory regarding the stacked layers lacks chemical characterization and would be based solely on the morphology and thus remain inconclusive at this point.

Three multi-layered vascular grafts were fabricated in addition to aforementioned four single-layered grafts:

- PLCL-L grafts that have PLCL as the luminal layer and PDO as the exterior layer.
- PLCL-E grafts that have PLCL as the exterior layer and PDO as the luminal layer.
- PLCL-M grafts that have PLCL as the middle layer and PDO as both luminal and exterior layer.

The SEM images of their cross-sections showed that all of the three formulas exhibit severe delamination due to weak intermolecular adhesion, thus disqualifying their potential use as vascular grafts (Figure 2.6B).

2.3.4 Effects of Fast-Degrading PDO on *In Vivo* Cell Infiltration

To investigate the role of the fast-degrading polymer PDO in *in vivo* cell infiltration, the four single-layered vascular grafts (PLCL, 20% PDO, PLCL/PDO blend, and PLCL/PDO co-spun) were implanted subcutaneously into 2-month-old male SD rats. The grafts were explanted 2 and 4 weeks after implantation and H&E staining was performed to inspect cell infiltration. Results showed that at 2 weeks, all implanted vascular grafts had cells infiltrated (Figure 2.7A). The 15% PLCL grafts had the least cell infiltration, with the majority of the cells residing at the exterior rim of the grafts and few cells in the middle of the grafts. The 20% PDO grafts showed drastically higher numbers of cells residing throughout the grafts. As expected, the PLCL/PDO blend grafts, which exhibit morphology with combined features of 15% PLCL and 20% PDO, had a compromised number of cells within the grafts compared to 20% PDO grafts.

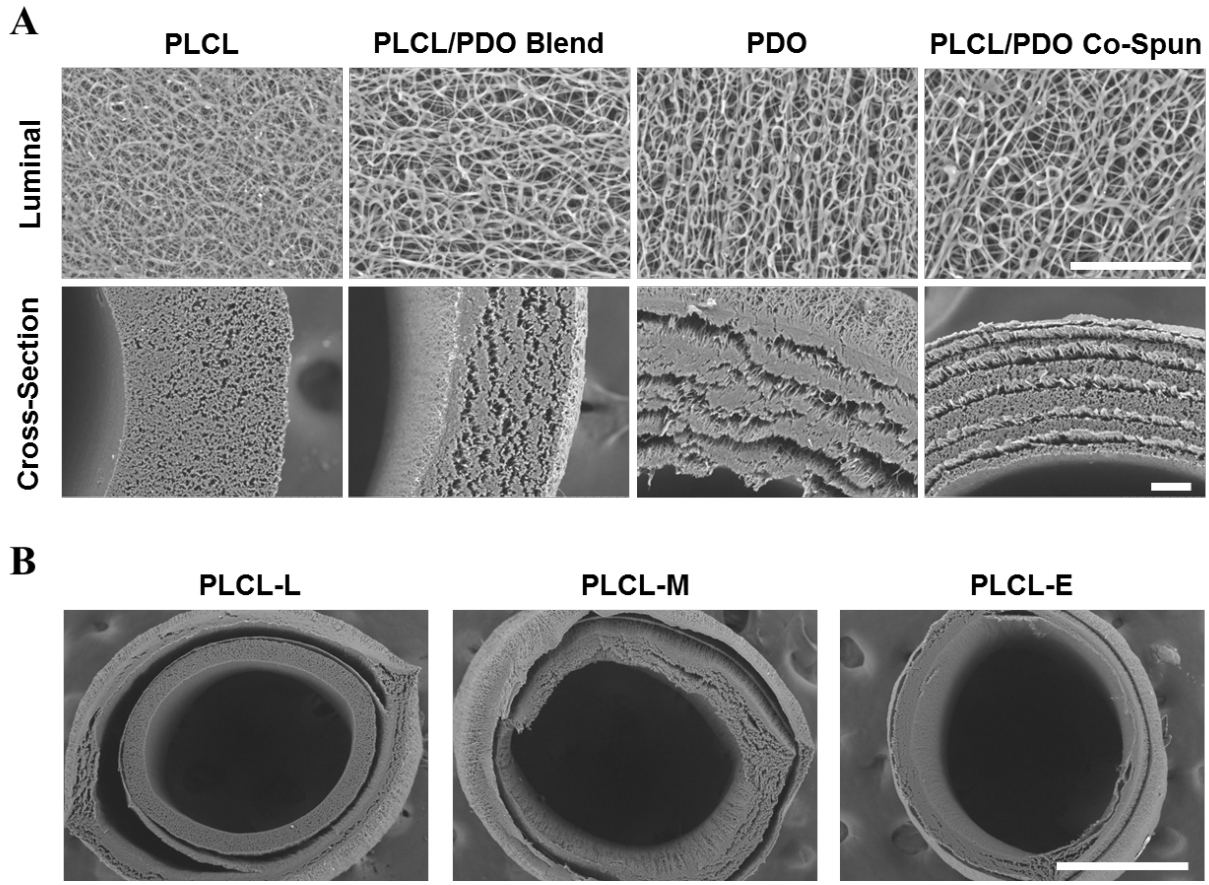

Figure 2.6 Characterization of single- and multi-layered vascular grafts. (A) Luminal (top) and cross-section (bottom) surface of single-layered vascular grafts electrospun with 15% PLCL, PLCL/PDO blend, 20% PDO, and PLCL/PDO co-spun. Scale bar = 50 μm. (B) Cross-section surfaces of multi-layered vascular grafts with the following structure: (left) PLCL as the luminal layer and PDO as the exterior layer; (right) PDO as the luminal layer and PLCL as the exterior layer; and (middle) PLCL as the middle layer and PDO as both luminal and exterior layer. Scale bar = 500 μm.

The PLCL/PDO blend, 20% PDO, and 15% PLCL grafts all exhibited a relatively uniform cell distribution. The PLCL/PDO co-spun grafts, on the other hand, showed a unique, interesting cell distribution pattern. As mentioned earlier, although PLCL and PDO have similar chemical structure, their properties differ slightly. One of the differences is manifested in their H&E staining appearance. The PLCL showed a clean and translucent staining, as shown in 15% PLCL graft, while the PDO stained yellowish and opaque, as shown in 20% PDO and PLCL/PDO blend grafts (Figure 2.7A). The PLCL/PDO co-spun grafts, on the other hand, had a non-uniformly colored staining. Similar to its morphological structure shown by SEM images, the grafts exhibited a stacked color pattern alternating with translucent and opaque layers, with the cells distributed exclusively in the opaque region of the grafts. This suggests that the PDO might have a beneficial effect on cell infiltration and attachment.

At 4 weeks, the amount of cells infiltrated was not obviously more than their 2-week counterparts (Figure 2.7B). This suggests the majority of the cell infiltration takes place shortly following subcutaneous implantation. At 4 weeks, 15% PLCL, PLCL/PDO blend, and co-spun grafts had maintained similar structural integrity as their respective 2-week samples. However, 20% PDO grafts had largely degraded and lost structural integrity.

Not only did cells infiltrate into grafts, but there was also tissue growing surrounding the implanted grafts. For subcutaneous implantation, the amount of tissue surrounding the grafts at 2 weeks and 4 weeks did not differ greatly. The 15% PLCL and PLCL/PDO blend grafts were relatively clean, with minimal tissue growing around the grafts. The PLCL/PDO co-spun grafts had moderate amount of surrounding tissue. In contrast, 20% PDO grafts triggered a strong cellular response with the thickest layer of tissue confining the grafts compared to the other grafts.

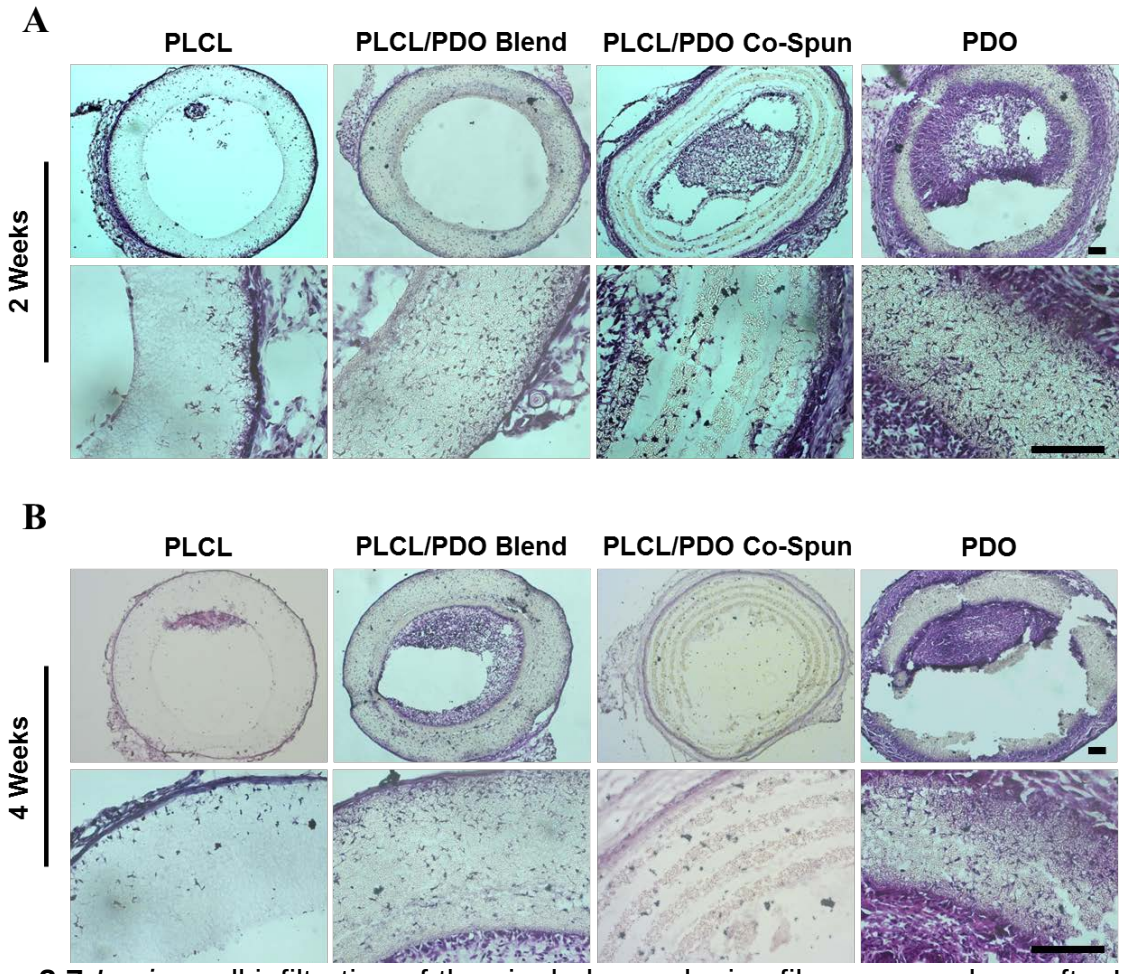

Figure 2.7 *In vivo* cell infiltration of the single-layered microfibrous vascular grafts. H&E staining of single-layered vascular grafts electrospun with 15% PLCL, 20% PDO, PLCL/PDO blend, as well as vascular grafts co-electrospun with PLCL and PDO at (A) 2 weeks and (B) 4 weeks after subcutaneous implantation. Scale Bar = 100μm.

2.4 Discussion

Cardiovascular disease, one of the leading causes of death, severely impacts a patient's well-being. A common treatment for vascular diseases is performing bypass surgeries with artificial vascular grafts. Therefore, there is a great need to develop a vascular graft with optimal mechanical and biochemical properties. In particular, the development of successful small-diameter vascular grafts (<5mm) remains challenging due to frequent thrombosis and occlusion. Many vascular grafts have been developed over the past decade. ePTFE is one of the materials that has been frequently used for commercial vascular grafts. However, ePTFE vascular grafts have an unsatisfactory *in vivo* performance on patency, despite heparin coating (36). In addition, tissue engineered grafts in general, both synthetic and decellularized native arteries, have limited host cell infiltration and remodeling even 6 to 12 months after implantation (18, 37-40).

The primary purpose of vascular grafts is to serve as a scaffold into which cells can adhere and grow. An ideal graft would provide the necessary mechanical strength to withstand arterial pressure; biochemical cues for cells to adhere and proliferate; structural support to physically anchor and secure neoarteries; and be able to degrade and be cleared from the system on timely order when the vascular regeneration is finished. In addition, a good vascular graft would allow wall remodeling by the infiltrated cells to obtain a desirable strength and elastic recoil. This cannot be achieved with a limited cell infiltration, highlights the need for such a vascular graft to be developed.

In this study, we investigated two approaches to enhance *in vivo* cell infiltration. The first approach increased vascular graft fiber spacing without post-electrospinning modification by modulating electrospinning parameters. The second approach introduced a fast-degrading polymer that degrades *in vivo* and leaves behind spaces for cells to infiltrate and proliferate as well as to encourage tissue regeneration.

Some common ways to increase graft pore size/fiber spacing involve using post-electrospinning modifications such as salt leaching and using sacrificial fibers. The principles of both methods are similar. The salt particles or sacrificial polymer are temporarily electrospun into the grafts with the base polymer. They are later removed using water or appropriate solvents, leaving behind empty spaces. However, one major drawback with these two methods is that the base polymer would collapse and partially fill the empty spaces (41). We, therefore, intend to fabricate vascular grafts with larger pore size/fiber spacing without any post-electrospinning modification. It has been reported that manipulating the electrospinning parameters would affect the properties of electrospun scaffolds. In particular, polymer solution flow rate and the distance from spinneret tip to collector both have a direct effect on fiber diameter and fiber spacing. It has been shown that to a certain extent, increasing the flow rate produces fibers with larger diameters, thus leading to larger fiber spacing (42). On the other hand, increasing the distance between spinneret and collector produces fibers with a smaller diameter and hence smaller fiber spacing (43). In this study, we modulated both the polymer solution flow rate and the distance between the spinneret and collecting mandrel

independently. It is surprising to see that modulating the flow rate of the PLCL polymer solution had no apparent effect on the fiber diameter and spacing. It is possible that the slowest flow rate tested in this study (1 mL/hr) has exceeded the upper limit of the effective range for PLCL. Reducing the distance between spinneret and mandrel marginally increased fiber diameter and spacing. Unfortunately, subcutaneous *in vivo* study showed no apparent difference in cell infiltration.

After failing to enhance cell infiltration using the first approach, we introduced a fast-degrading polymer in the second approach. A fast degrading polymer would shorten host exposure to the foreign materials and allow rapid host remodeling. For instance, researchers have developed a vascular graft with PCL and a fast-degrading elastomer poly (glycerol sebacate) (PGS) (44). The graft consists of a PGS core that was fabricated with salt fusion and leaching method, and a PCL sheath that was electrospun onto the PGS core. The graft degrades rapidly *in vivo* and allows the formation of neoarteries that are nearly free of foreign materials in 3 months. Although PGS is a promising candidate, it is difficult to work with technically. PGS requires gentle handling due to its low tensile strength. Moreover, electrospinning PGS is challenging because crosslinked PGS is insoluble in the organic solvent, which makes the use of uncrosslinked PGS prepolymer necessary. However, the glass transition temperature of PGS prepolymer is below room temperature, which causes the polymer to flow and electrospun fibers to fuse into a nonporous structure at room temperature. This fiber fusion is aggravated by the high temperature required for thermal crosslinking (45). Given these technical challenges, in this study, we used a different fast-degrading polymer, PDO. It is easy to handle and compatible with electrospinning, and is readily dissolvable in Tris-HFIP (the optimized solvent for PLCL according to laboratory protocols).

In this study, we developed 3 multi-layered vascular grafts using fast-degrading PDO and slow-degrading PLCL. Our preliminary *in vitro* results showed that PDO grafts lost the majority of the mechanical strength within a month, which is less than the time it takes to fully regenerate a neoartery. At least a layer of the vascular graft needs to stay in place to provide structural support while the arteries are regenerating. We, therefore, developed 3 multi-layered vascular grafts with the slower degrading PLCL as the luminal, middle, and exterior layer. Unfortunately, these multi-layered vascular grafts failed to provide structural integrity. Although PLCL and PDO share similar properties, their electrospun fibers do not have strong adhesion to each other. All the multi-layered vascular grafts exhibited severe delamination, which would be destructive for vascular grafts. As a result, the multi-layered vascular graft designs were excluded from the subsequent *in vivo* study.

Using PLCL and PDO, we have also developed 4 single-layered vascular grafts. Compared to PLCL grafts, PDO grafts exhibit larger pore size and fiber spacing, a potentially beneficial factor. Unfortunately, PDO grafts do not exhibit the desirable mechanical strength and structural integrity. The *in vivo* results showed that PDO grafts did recruit more cells but exhibited severe degradation 4 weeks after *in vivo* implantation, which is consistent with the preliminary observation. Since vascular

regeneration, in general, requires longer than 4 weeks, PDO grafts do not meet the timeframe requirement. In addition, rapid degradation is not entirely beneficial for vascular regeneration. Typically, faster degrading materials trigger more pronounced inflammatory reaction than slower degrading counterparts (46, 47), indicating that a balance between cell infiltration and degradation rate is mandatory. Among the single-layered vascular grafts tested, the balance is best reached by the PLCL/PDO blend grafts, which had moderate uniform cell infiltration and little cellular response. Based on the results of this study, the PLCL/PDO blend grafts will be used for the following research.

Although PLCL/PDO co-spun grafts did not have desirable *in vivo* cell infiltration, we have made an interesting observation. The SEM images showed that they possess distinct layers, presumably alternating layers of PLCL and PDO. The H&E staining of explanted grafts showed infiltrated cells residing in alternating layers as well. This suggests that limited cell infiltration in PLCL grafts is possibly due to lack of cell adhesion sites in addition to small pore size. Although PLCL exhibits desirable elastic and mechanical properties, the hydrophobicity of PLCL negatively influences protein adsorption, which in turn prevents the cells from adhering (48). Although PDO is also considered a hydrophobic material, it has more polar structures than PLCL, which in theory should be beneficial for cell adhesion. Therefore, it is possible that the enhanced cell infiltration in PDO compared to PLCL is attributed to a combination of decreased hydrophobicity and increased degradation rate.

In this study, we developed a working vascular graft with satisfactory subcutaneous *in vivo* performance. Because the subcutaneous environment differs significantly from the actual vascular environment, additional *in vitro* characterization and *in vivo* vascular implantation studies were carried out, and are discussed in detail in the next chapter.

Chapter 3: The Effect of Stromal Cell-derived Factor-1α on Endothelialization and Remodeling of a Cell-free Biodegradable Vascular Graft

3.1 Introduction

3.1.1 Blood Vessel Anatomy

Blood is transported through the body via blood vessels. An artery is a blood vessel that conducts blood away from the heart, and a vein is a blood vessel that carries blood toward the heart. Arteries and veins transport blood in two distinct circuits: the systemic circuit and the pulmonary circuit. Systemic arteries transport oxygenated blood to the body's tissues. The deoxygenated blood returns to the heart through systemic veins. In comparison, pulmonary arteries conduct deoxygenated blood to the lungs for gas exchange, and the freshly oxygenated blood is transported from the lungs to the heart through pulmonary veins. The common carotid arteries are systemic arteries that carry oxygenated blood to head and neck (49).

Different types of blood vessels have different functions and thus differ structurally, but they share common features. All vessels have a lumen, a hollow space inside the vessels through which blood flows. When a blood clot or thrombus is formed inside the lumen, blood flow is obstructed, resulting in a compromise in tissue oxygenation. This lack of oxygen supply may lead to tissue ischemia under severe conditions as oxygen is an essential element for the survival of cells/tissues. The undesirable process of thrombus formation is called thrombosis (49).

The blood vessel walls have three distinct tissue layers. From the outermost to the innermost, these three layers are called tunica adventitia, tunica media, and the tunica intima, respectively. These three tunica layers are primarily comprised of living cells and their secretory products such as collagenous and elastic fibers. The tunica adventitia consists of connective tissue, mostly collagenous fibers. This tunica adventitia layer is not very distinct but rather blends with the surrounding connective tissue. It aids in securing the blood vessel in a relative position within the body so that physical movement does not move the blood vessel and hence disrupt blood flow (49).

The middle layer of the blood vessel wall is tunica media. Smooth muscle cells (SMCs) and elastic/collagenous fibers predominate in the tunica media layer. In response to a change in body conditions, smooth muscle cells can regulate blood flow and blood pressure by either contracting or relaxing. When smooth muscle cells contract, the blood vessel lumen narrows, resulting in increased blood pressure and reduced blood flow. Similarly, when smooth muscle cells relax, the lumen widens, resulting in reduced blood pressure and increased blood flow. This blood pressure/flow regulation by smooth muscle cells is specifically important in arteries (49).

The most interior layer is named tunica intima, which consists of epithelial and connective tissue layers. The endothelium, a thin layer of specialized simple squamous

epithelial cells named endothelial cells (ECs), lines the tunica intima. Endothelium is continuous throughout the entire vascular system. Vascular endothelia cells serve many crucial purposes. For instance, vascular endothelial cells can release chemicals that constrict the smooth muscle cells to increase blood pressure. Endothelium also produces anticoagulant such as heparin sulfate, and hence providing a non-thrombogenic surface. Damage to the endothelium and exposure of the underneath collagenous fibers to blood is one of the primary causes of thrombosis (49).

3.1.2 Host Response

As discussed in the previous chapter, there are two approaches to making substitutes for native arteries: the use of natural and/or synthetic materials. Natural materials have the advantages of being native, biocompatible to the patient, having limited immune rejection, and optimal biological, structural, and mechanical properties. Unfortunately, its availability on demand remains a major challenge. Synthetic materials have the advantages of high reproducibility, availability, and we can fine-tune the manufacturing process to produce biomaterials with desirable properties. However, one major disadvantage of using synthetic materials is the risk of immune rejection by the host.

Synthetic implants are foreign materials to living tissues. Implantation of such an artificial device in combination with any tissue injury that may occur during the surgery could trigger a cascade of inflammatory responses followed by wound healing and foreign body reaction (50). Both physical and chemical properties of the device, including composition, contact duration, degradation rate, morphology, porosity, roughness, shape, size, sterility and surface chemistry, would determine the degree and extent of the foreign body reaction (51-53). Following a surgical implantation, there is usually initial nonspecific blood/protein-device interaction that brings about an initial acute inflammatory phase and a subsequent chronic phase (50, 52, 54).

During the initial acute phase, blood vessels dilate to allow excess blood flows into injury sites. Cytokines and growth factors are released, and leukocytes adhere and infiltrate into the injury sites. Monocytes are recruited to the injury sites as well, where they differentiate and mature into macrophages. The purpose of this initial acute phase is mostly cleaning of the wound site; this phase generally lasts from hours to days (55-60).

Initial acute inflammation would transit into chronic inflammation when foreign stimuli are persistent, such as a continual presence of the foreign biomaterials (50). This phase is generally characterized by the presence of monocytes and macrophages, as well as angiogenesis and proliferation of connective tissue to remodel the injured area (57-61). In particular, angiogenesis, the formation of blood vessels, plays a crucial role in wound healing as it allows transportation of necessary nutrients to the damaged tissue sites (62). The end stage of foreign body reaction involves encapsulation of the implanted device by a vascular and collagenous fibrous tissue that is typically 50-200μm thick. This fibrous encapsulation is inevitable even for inert biological biomaterials,

which lack functional biological domains and therefore trigger minimal immune responses. Fibrous encapsulation confines the implanted device and consequently impedes the tissue-device interaction (58, 61, 63, 64). As a result, excessive fibrous encapsulation is often considered a sign of and mechanism for implant failure.

3.1.3 Role of Immune Cells

Role of Leukocytes

White blood cells or leukocytes are the essences of the immune system. Both innate and adaptive immune responses depend upon the activities of leukocytes. These cells originate from the bone marrow and migrate to the peripheral tissues. They are found both within tissues or circulating in the bloodstream. Leukocytes can be further divided into three categories: polymorphonuclear leukocytes, lymphocytes, and monocytes (65).

Polymorphonuclear leukocytes include neutrophils, eosinophils, and basophils. Polymorphonuclear leukocytes are produced during immune responses, and they are all relatively short-lived. When infection or inflammation occurs, polymorphonuclear leukocytes migrate to affected sites from the blood stream. Neutrophils are the most abundant and important cells in innate immunity. They are phagocytic, i.e., they engulf a variety of microorganisms and degrade them enzymatically. Eosinophils and basophils are important for their defensive role against parasites, which are too large to be taken up by neutrophils. They contain various enzymes and toxic proteins, which are released when they are activated (65).

Lymphocytes include three major classes: B and T lymphocytes, as well as natural killer cells. B and T lymphocytes play essential roles in adaptive immunity, where they function in antibody- and cell-mediated adaptive immunity, respectively. In comparison, natural killer cells are responsible for innate immunity. They are cytotoxic and have the ability to recognize and destroy abnormal cells such as virus-infected and some tumor cells (65).

Monocytes circulate in the bloodstream and continually migrate into tissues, where they differentiate and mature into their final macrophage form (65).

Role of Macrophages

Macrophages play a central and essential role in the immune response. They serve as an antigen presenter to lymphocytes, as well as supportive cells in the replication of lymphocytes. Additionally, macrophages serve as fundamental protective cells to ingest and kill invading foreign organisms. Macrophages release an enormous number of factors involved in host defense and inflammation. During infection, macrophages transit from a normal resting form into “activated macrophage” through a cell-mediated immunity. Activated macrophages differ from resting macrophages morphologically, functionally, and metabolically. They possess increased ability to

undergo phagocytosis and pinocytosis, processes to engulf other cells or particles, and internalize soluble materials, respectively (65).

Traditionally, defensive cellular responses of macrophages initiated by biomedical devices are considered detrimental due to their phagocytic activities and contribution to the host inflammatory response. However, over the past decade, it has been discovered that macrophages exhibit a spectrum of polarization states. At one end of the spectrum, there is the pro-inflammatory, cytotoxic M1 “fighting” phenotype characterized by cells that promote pathogen elimination and contribute to inflammation. In contrast, the anti-inflammatory M2 “fixing” phenotype on the other end of the spectrum plays a pivotal role in immunomodulation, tissue repair, and remodeling (66-68).

All inflammations involve a mixture of M1 and M2 responses. It has been suggested that a high M2:M1 ratio results in better remodeling (69). However, prolonged M2 expression may lead to the formation of detrimental foreign body giant cells (64). Interestingly, macrophages can sense their microenvironmental cues, both biochemical and biophysical, and switch their polarization states in response. For instance, it has been shown that there is a positive correlation between the fiber/pore size of an electrospun polydioxanone scaffold and the M2:M1 ratio of the macrophages seeding atop (70). Therefore, maintaining an optimal M2:M1 ratio for an appropriate duration by modulating biochemical and biophysical properties of a biomedical device is the key to successful tissue remodeling.

3.2 Materials and Methods

3.2.1 Fabrication and Characterization of Vascular Grafts

Fabrication of Vascular Grafts

PLCL/PDO blend vascular grafts were fabricated as described in Section 2.2.1.

Characterization of Vascular Grafts

The overall fibrous structure of electrospun vascular grafts was examined and imaged using a SEM (Hitachi TM-1000). In addition, to determine the mechanical properties of the electrospun vascular grafts, graft ring segments of 1mm in diameter and 2 mm in longitudinal width were prepared and subjected to uniaxial tensile testing in the radial direction. In detail, two 0.3-mm-diameter stainless steel wires (McMaster-Carr) were inserted through the lumen of the ring segment and fixed on mechanical loading grips. The ring segment was deformed until failure as the two wires were pulled in opposite uniaxial direction at a rate of 0.1mm/sec. The applied force and corresponding deformation were recorded. The Young's modulus was calculated based on the applied force, deformation, and dimensions (thickness and longitudinal width) of the graft ring segments. The peak stress prior to failure was noted as the ultimate tensile strength.

Degradation of Vascular Grafts

Degradation of vascular grafts caused by hydrolysis was measured by mass loss. The PLCL/PDO blend grafts were cut into 1cm long conduits. The weight of each conduit sample was measured before the degradation assay. To degrade the grafts, the conduit samples were placed in PBS. During the degradation study, the samples were kept at 37^{o}C on a shaker maintained at 120 rpm to mimic the physiological flow condition. To avoid random local hydrolytic degradation resulting from acidic polymer remnants, PBS was used in an excess amount and changed daily throughout the study. Samples were collected after 7, 14, 21, and 28 days of degradation. The samples were washed with water to remove residual salt particles and vacuum dried overnight. The weight of the samples at each time point was measured using a precision scale. The percentage degraded was calculated using following equation:

$$\%\ Degradation = \frac{(w_o - w_t)}{w_o}$$

In addition, ultimate tensile strength of post-degraded samples was measured at each time point as well.

3.2.2 Heparin Conjugation

Heparin conjugation and quantification were performed by collaborator Yu-Fang Angela Hsieh, a Ph.D. Candidate from Song Li Lab, UC Berkeley. In brief, a two-stage

(ammonia followed by hydrogen) plasma treatment was used to introduce amine functional groups on the surface of PLCL/PDO blend grafts. The plasma-treated grafts were incubated with a heparin solution in cyanoborohydride coupling buffer overnight. The amount of free amine groups on the plasma-treated grafts, the amount of heparin conjugated to the grafts, and anti-thrombogenic activity of heparin were quantified with Orange II, Toluidine Blue, and Anti-thrombin-III assay, respectively (data not shown).

The uniaxial tensile test was performed on plasma-treated and heparinized grafts in the radial direction. Ultimate tensile strength of each sample was measured and compared to untreated grafts. In addition, hydrolytic degradation was performed on heparinized grafts following protocol described in Section 3.2.1. Mass loss percentage and ultimate tensile strength of post-degraded samples were measured at each time point and compared to untreated grafts.

3.2.3 SDF-1α Immobilization and *In Vitro* Release

SDF-1α Immobilization and Quantification

To immobilize SDF-1α onto the grafts, heparinized grafts were incubated with SDF1α (500 ng/mL) in PBS overnight at 4^{o}C to foment its binding to heparin and hence immobilization onto the grafts. To quantify the amount of SDF-1α initially loaded onto the grafts, the grafts were removed from the solution, and ELISA was performed to measure the concentration of unbound SDF-1α. The amount of SDF-1α immobilized onto the graft was calculated based on the concentration of initial and unbound SDF-1α. The plasma-treated blend vascular graft was used as a control to measure the amount of SDF-1α passively absorbed onto the grafts.

In Vitro Release of SDF-1α

The *in vitro* release of immobilized SDF-1α was evaluated under static conditions over a period of 7 days. The SDF-1α immobilized heparinized grafts were removed from SDF-1α solution and placed in 1mL of PBS. The grafts were kept at 37^{o}C in an incubator under static conditions. At the end of 1, 4, and 7 days of incubation, the grafts were removed from the solution, and the amount of released SDF-1α in the supernatant was quantified using an ELISA kit.

3.2.4 Implantation and Explantation of Vascular Grafts

The left common carotid artery was dissected, clamped, and transected. The vascular graft was sutured end to end using a 9-0 needle. To determine patency of the graft at the time of explantation after 2 weeks and 2 months *in vivo*, the blood flow in the blood vessel at the distal end of the graft in the live animal under anesthesia was examined. To elaborate, forceps were used to hold distal blood vessel near the anastomotic site while distally attached native carotid artery was dissected. The forceps were subsequently released to determine whether unobstructed blood flow was passing through the graft. The graft was defined as being patent only if blood flow and

noticeable pulsation were observed through the graft. Lastly, the animals were euthanized. The vascular grafts were explanted and prepared for histological analysis, immunohistochemistry, and *en face* immunofluorescence staining.

3.2.5 *En Face* Immunofluorescence Staining

Each explanted graft was cut into 4 slices along the longitudinal direction using microscissors. The samples were fixed with 4% PFA for 30 minutes, washed with PBS, and blocked with 4% donkey serum for an hour. Samples were incubated with primary antibodies against endothelial progenitor cell (EPC) marker CD34 and EC marker CD31. The samples were then washed with PBS and incubated with Alexa-Fluor 488 or Alexa-Fluor 546 labeled secondary antibodies and Hoechst 33342, followed by confocal microscopy.

3.2.6 Histological Analysis and Immunohistochemistry

As described in Section 2.2.5, the grafts were explanted and fixed with 4% PFA and dehydrated with sucrose. The grafts were subsequently frozen in an OCT compound and sectioned into 10μm-thick slices using a cryostat. H&E staining was subsequently performed as described in Section 2.2.5.

Immunohistochemistry

The slides were fixed with 4% PFA for 15 minutes, followed by permeabilization with 0.5% triton-100 for 10 minutes. The slides were blocked with 4% donkey serum in PBS for an hour and incubated overnight at 4^{o}C with primary antibodies against EC/EPC markers CD31 and CD34; SMCs markers αSMA and CNN1; and immune cell markers CD68, CD163, and CD11b (Table 3.1). The samples were then washed with PBS and incubated with Alexa-Fluor 488 or Alexa-Fluor 546 labeled secondary antibodies and Hoechst 33342, followed by fluorescent microscopy.

Antibody	Company	Catalog #	Dilution
CD31	Abcam	ab28364	1:50
CD34	R&D Systems	AF4117	1:40
αSMA	Abcam	ab5694	1:100
CNN1	Abcam	ab46794	1:100
CD68	AbD Serotec	MCA341R	1:100
CD163	Santa Cruz	sc-58965	1:50
CD11b	Abcam	ab8879	1:100

Table 3.1 Antibody information for immunohistochemistry.

Alizarin Red S Staining

Slides were fixed with 4% PFA for 15 minutes and rinsed with water. Fixed slides were incubated with Alizarin Red S working solution (2% w/v alizarin red S in di-water,

pH 4.1~4.3) for 45 minutes and subsequently washed with water. Phase-contrast images were captured with Zeiss microscope.

3.2.7 Statistical Analysis

Student's t-test was performed to detect whether a significant difference exists between two sample groups. For multiple sample comparison, analysis of variance (ANOVA) was used first to detect whether or not there was a significant difference among the groups; Holm's t-test was subsequently performed on all possible pairs to isolate the different sample. A p-value of 0.05 or less was considered to have a significant difference.

3.3 Results

3.3.1 Characterization of Microfibrous Vascular Grafts with SDF-1α

Microfibrous vascular grafts were fabricated by electrospinning the aforementioned PLCL/PDO blend polymer solution. Electrospun vascular grafts underwent a two-stage ammonia plasma treatment to adhere amine functional groups, which were subsequently used to conjugate to heparin, onto the surface of the grafts. To characterize the mechanical properties of the vascular grafts, a uniaxial tensile test in the radial direction was performed on the grafts. Untreated grafts have an elastic modulus of 1.24±0.08 MPa (Figure 3.1A). Although the electrospun vascular graft is less elastic than native arteries, which have an elastic modulus of 3.66±0.25 MPa, the elastic modulus of the grafts is on the same order of magnitude as native carotid arteries. Neither the ammonia plasma treatment nor heparinization significantly modified the mechanical properties of the grafts: elastic moduli of plasma-treated and heparinized grafts are 1.26±0.19 and 1.34±0.13 MPa, respectively. In addition, the untreated, plasma-treated, and heparinized grafts have comparable ultimate tensile strengths of 7.81±1.11, 7.98±0.71, and 7.90±1.13 MPa, respectively, with no significant difference (Figure 3.1B).

Mass loss and ultimate tensile strength loss were studied over 4 weeks of *in vitro* hydrolytic degradation, which was carried out in PBS at 37^{o}C on a shaker maintained at 120 rpm to mimic the physiological *in vivo* flow condition. The untreated PLCL/PDO blend grafts lost approximately 8% of their original mass over the 4-week period in PBS (Figure 3.2A). However, their mechanical properties changed drastically: the ultimate tensile strength of untreated grafts is only 20% of their pre-degraded counterparts, as shown in Figure 3.2B. Heparinization has made the grafts more prone to hydrolysis. After 4 weeks of degradation, the heparinized grafts lost approximately 12% of their original mass and 80% of their ultimate tensile strength. Moreover, at any point throughout the degradation, heparinized grafts had less mass remaining and weaker ultimate tensile strength compared to untreated grafts.

To immobilize SDF-1α onto the grafts, heparinized grafts were incubated overnight with SDF-1α (500 ng/mL) in PBS. Quantification by ELISA showed that the initial loading of SDF-1α onto heparinized grafts by SDF-1α-heparin interaction or plasma-treated grafts by passive absorption are comparable: at 52.78±7.22% and 55.05±5.36%, respectively (Figure 3.1C). The stability and static *in vitro* release of SDF-1α were also examined (Figure 3.2C). The SDF-1α immobilized on heparinized grafts is stable and released relatively slowly. It has a burst release over the first 24 hours and a steady release afterward. After 7 days of release, there was approximately 90% of initially immobilized SDF-1α remaining on the heparinized graft. In comparison, the SDF-1α passively absorbed onto plasma-treated grafts is less stable and released relatively rapidly. Approximately 70% of initial passively absorbed SDF-1α remained on the plasma-treated graft after 7 days of *in vitro* release.

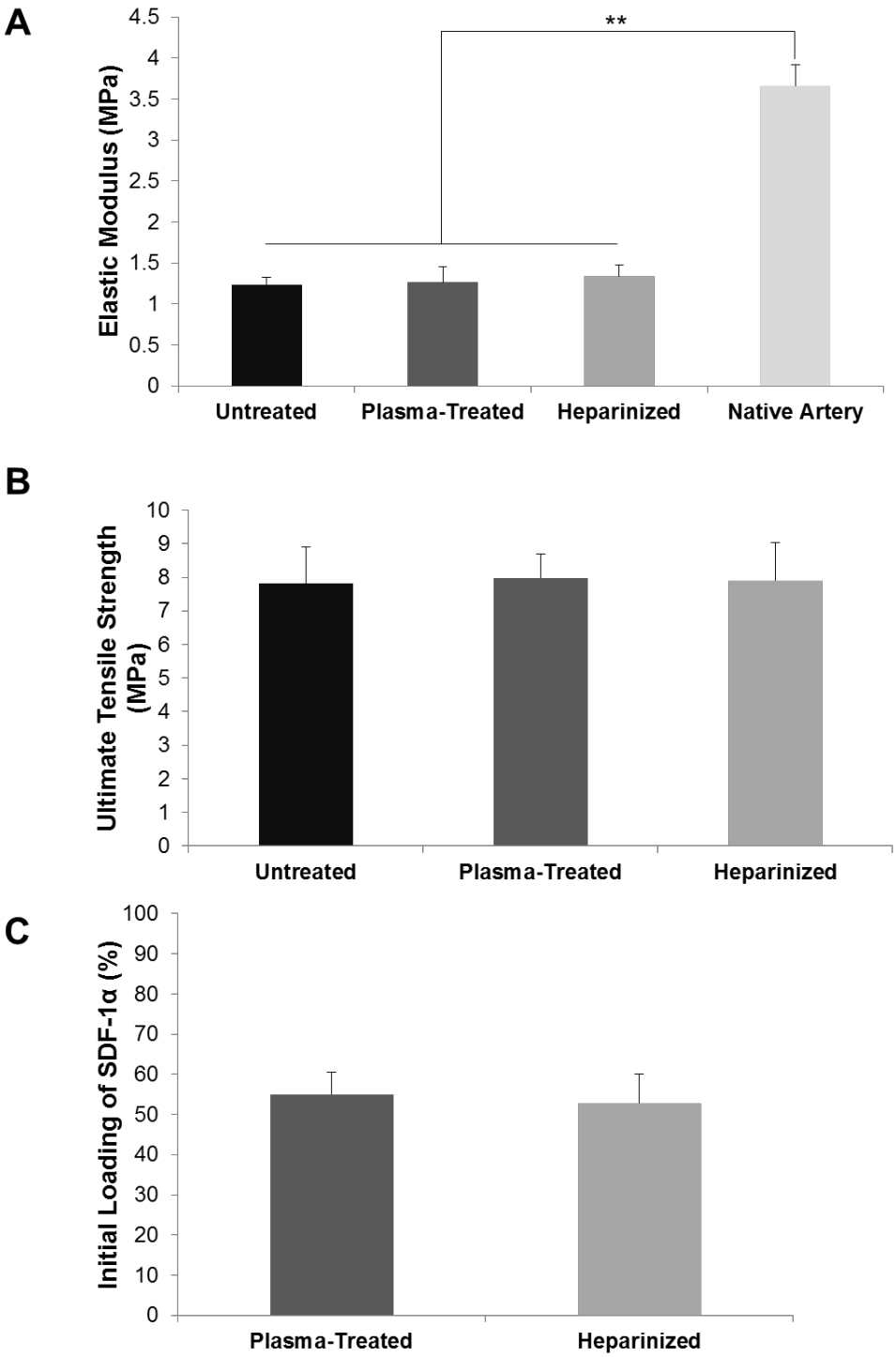

Figure 3.1 Mechanical and chemical characterization of microfibrous vascular grafts. (A) Elastic moduli of untreated, plasma-treated, heparinized vascular grafts, and native common carotid arteries. (B) Ultimate tensile strength of untreated, plasma-treated, and heparinized vascular grafts. (C) Initial loading of SDF-1α immobilized onto plasma-treated and heparinized vascular grafts. ** $p<0.01$, (n=3)

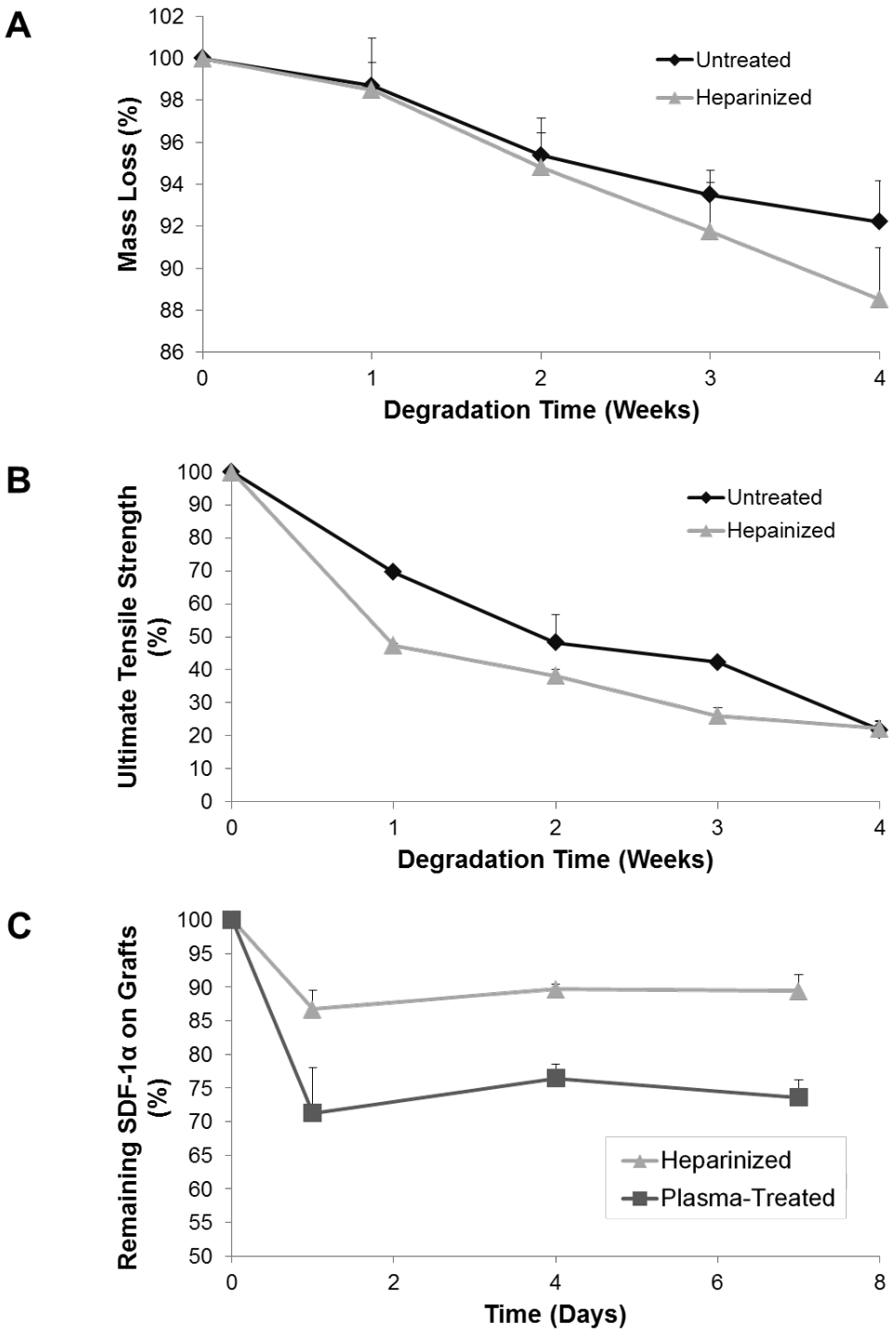

Figure 3.2 Mechanical property changes during hydrolysis and release of SDF-1α. (A) Mass loss of untreated and heparinized vascular grafts during 4 weeks of hydrolysis in PBS under constant agitation. (B) Changes in the ultimate tensile strength of untreated and heparinized vascular grafts during 4 weeks of hydrolysis in PBS under constant agitation. (C) The time course of SDF-1α release from plasma-treated and heparinized grafts under static condition. (n=3)

3.3.2 Morphology and Patency of Vascular Grafts

To evaluate the performance of PLCL/PDO blend grafts and the effect of SDF-1α *in vivo*, heparinized grafts with and without immobilized SDF-1α were implanted into the left common carotid artery of 2-month-old male SD rats by anastomosis. The implanted grafts were 1cm long with an inner diameter of 1mm. Grafts were examined 2 weeks and 2 months after implantation. 6 animals were used per group per time point (n=6 x 4 = 24). All animals survived the surgery, and 22 animals survived until the end of the study. Unfortunately, 2 rats from the SDF-1α group died, one from each time point, potentially due to the surgery complications.

Two weeks after implantation, micro-vessels were observed in the tissue surrounding the grafts for both the heparin and heparin-SDF-1α groups (Figure 3.3A). There was evidence of greater surrounding tissues growth around the heparin-SDF-1α grafts, suggesting a better integration of the graft into the native tissue than heparinized grafts. Despite the tissue growth on the exterior surface, H&E staining demonstrated that there was little cell infiltration into the grafts for both groups at 2 weeks. All patent grafts had a wide opening lumen with a layer of cells adhering onto the luminal surfaces that had potentially migrated from the adjacent blood vessels or recruited from the streaming blood. There were, however, occluded grafts from both heparin and heparin-SDF-1α groups. Immunofluorescent staining of the occluded grafts showed that the cells in the clogs were positive for CD45, which is a marker for leukocytes, suggesting thrombosis is the primary reason jeopardizing patency of the vascular grafts at an early stage (data not shown).

Two months after implantation, vascular grafts from both the heparin and heparin-SDF-1α groups had integrated further into the native tissue (Figure 3.3B). The amount of tissue growing around the grafts increased compared to their respective 2-week samples. Between the two groups, more tissue growth was observed on the heparin-SDF-1α grafts. Patency study showed that 17% (1 of 6) of heparinized grafts and 80% (4 of 5) of SDF-1α immobilized grafts were patent at 2 months after implantation, suggesting that SDF-1α immobilization improves long-term patency. The H&E staining demonstrated that the sole patent heparinized graft had a narrowed lumen, which was caused by extensive neointimal formation. In addition, immunofluorescent staining showed that expression of CD45 in cells amidst the clogging had disappeared, suggesting that vessel narrowing could be the major mechanism for vascular graft occlusion in the long term. At 2 months, PLCL/PDO blend grafts had partially degraded and were replaced by infiltrated cells for both heparin and heparin-SDF-1α groups. Although SDF-1α immobilized grafts did not have lumen narrowing as great as the heparinized group, a thin layer of neointima formed, suggesting that the SDF-1α might have improved patency by regulating cell recruitment and/or proliferation.

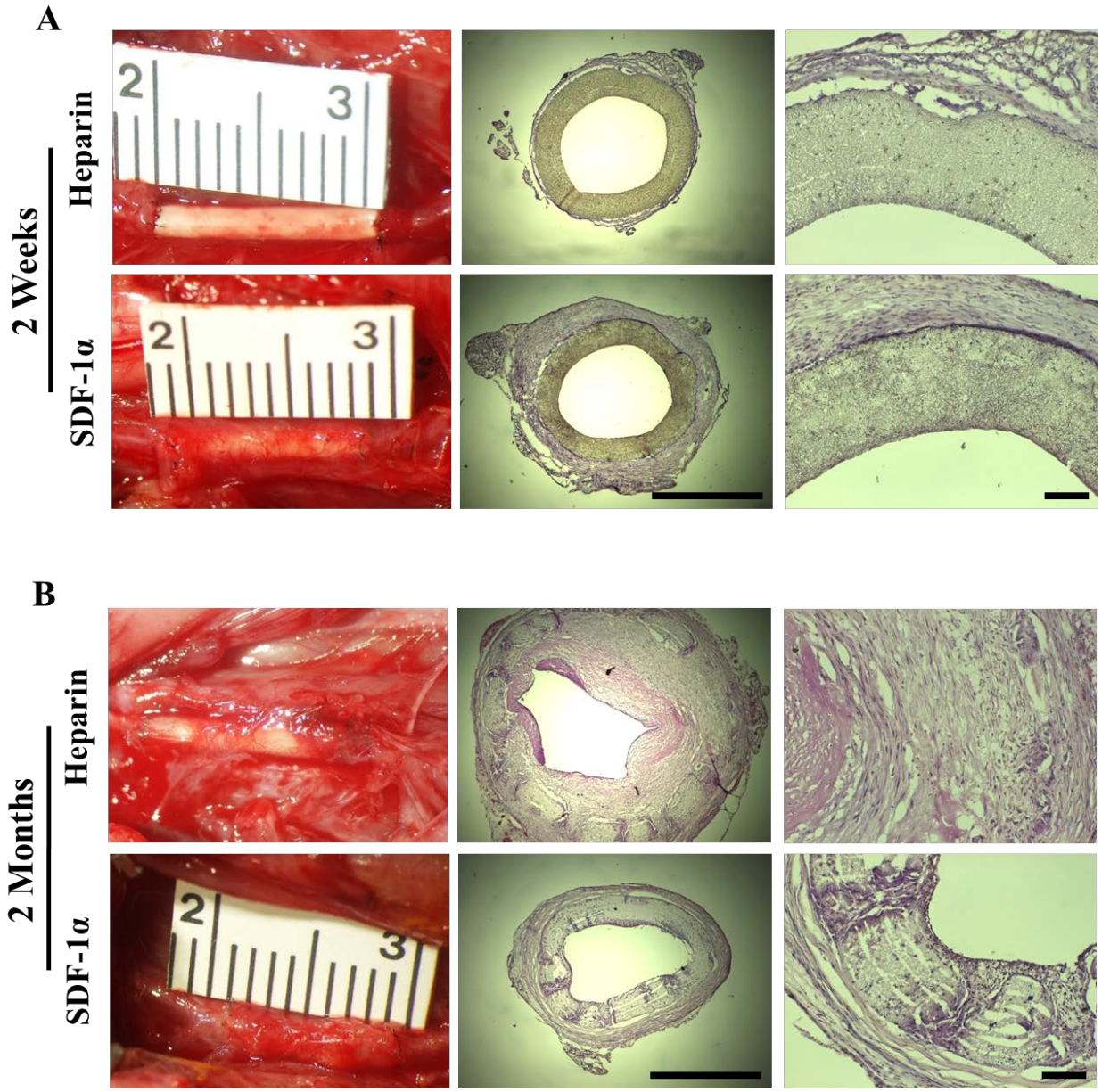

Figure 3.3 Tissue ingrowth and cell infiltration of vascular grafts. Vascular grafts explanted at (A) 2 weeks and (B) 2 months for heparinized (top), and SDF-1α immobilized (bottom) group. Representative images of grafts *in situ* taken immediately prior to explantation (left) and H&E staining of the cross-section of explanted grafts at low (middle, scale bar = 1mm) and high (right, scale bar = 100μm) magnification.

3.3.3 EPC Recruitment and Endothelialization

To identify the cells lining the luminal surfaces of the grafts, *en face* and cross-section immunofluorescent staining against EC marker CD31 and EPC marker CD34 was performed on both the heparin and the heparin-SDF-1α groups. Hoechst staining of the cross-section of 2-week samples from both groups showed that more cells were observed within the grafts near the anastomotic ends than the mid-graft region. In addition, no noticeable difference in cell number was observed between the distal and the proximal end of the vascular graft (data not shown). This suggests that cells within the grafts might have migrated from adjacent native carotid arteries, and blood flow direction is not a determinative factor for cell migration into the grafts. A comparison between heparin and the heparin-SDF-1α groups demonstrated no apparent difference in the number of cells at either anastomotic ends or the mid-graft region.

En face staining of heparinized grafts at 2 weeks showed that cells expressing both CD31 and CD34 were observed near anastomotic ends of the grafts (Figure 3.4A). Although the cells had a well-defined cell-cell boundary, the cells were not aligned in the direction of blood flow as is the case in native blood vessels; this suggests these cells are still in the process of remodeling. In addition to anastomotic ends, patches of CD31 and CD34 double positive cells were found throughout the grafts. These findings suggest that heparinized PLCL/PDO blend grafts are capable of recruiting CD31 and CD34 positive cells both from adjacent carotid arteries and circulating bloodstream. Cross-section staining of 2-week graft samples showed no difference in marker expression of CD31 and CD34 in cells lining the luminal surfaces between heparin and the heparin-SDF-1α groups (Figure 3.4B). However, in the tissue surrounding the grafts, more microvasculature structures were observed in the heparin-SDF-1α group, demonstrating the angiogenetic ability of SDF-1α.

At 2 months after implantation, the luminal surfaces of all patent grafts were almost completely covered by cells, including the regions that experienced partial degradation (Figure 3.4B). Cross-section immunofluorescent staining showed most cells were double positive for CD31 and CD34 for both heparin and the heparin-SDF-1α groups, suggesting that EPCs were not done differentiating into terminal ECs. In the tissue surrounding the heparinized grafts, few CD31 positive cells were detected. However, it is surprising to find a weak signal of CD34 still expressed in these cells at 2 months after implantation. In contrast, in the tissue around the heparin-SDF-1α grafts, a greater number of cells had strong CD34 expression. In addition, CD31 positive cells were observed in the microvessels in the surrounding tissue; further demonstrating abilities of SDF-1α to promote initiation of angiogenesis and blood vessel maturation.

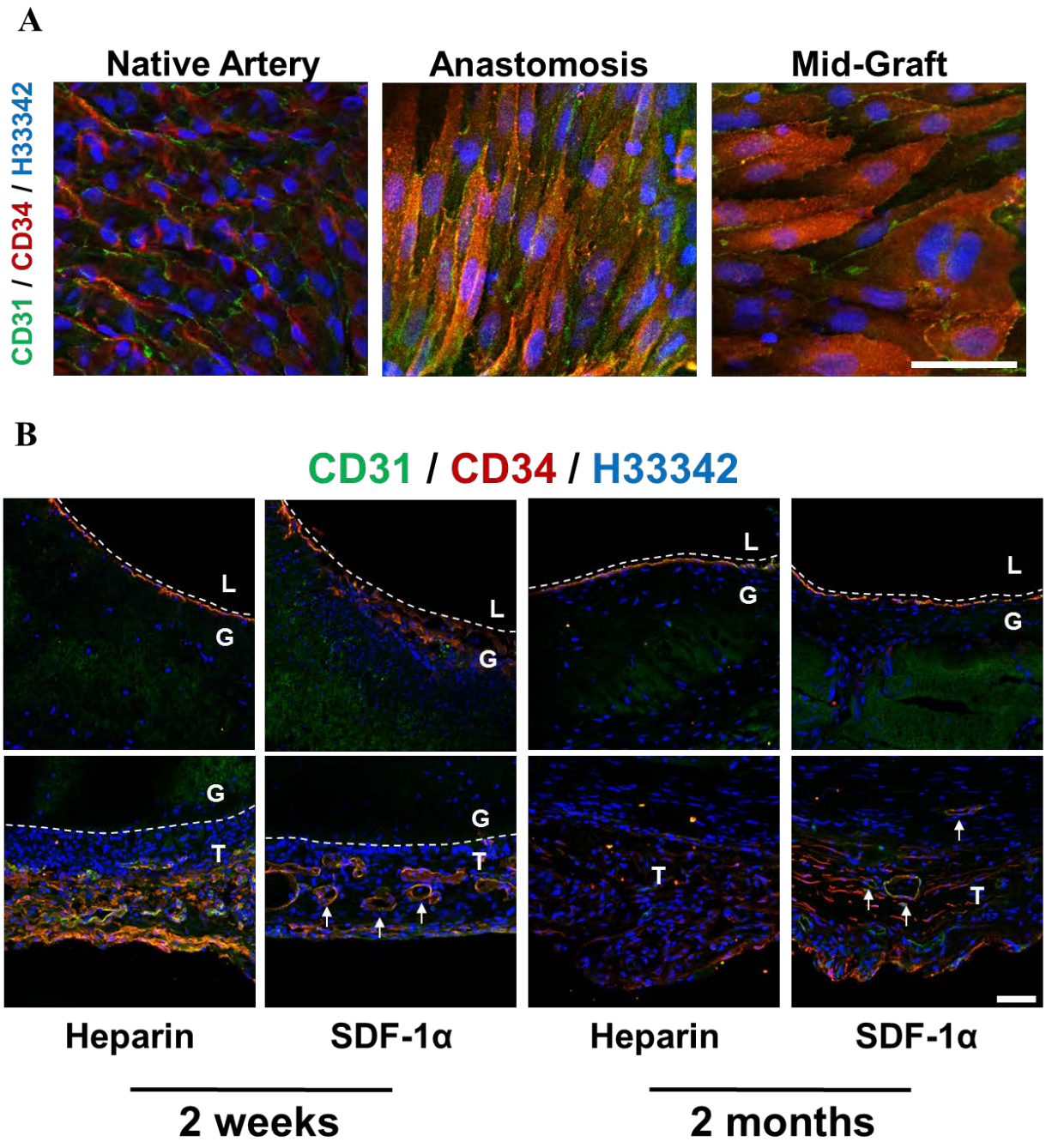

Figure 3.4 Identification and characterization of ECs and EPCs. (A) *En face* immunostaining for CD 31 (green) and CD34 (red) of the native artery (left), and heparinized vascular grafts at 2-week after implantation at anastomotic (middle) and mid-graft (right) sites. (B) Immunostaining for CD 31 (green) and CD34 (red) of the cross-section of heparinized and SDF-1α immobilized grafts at 2 weeks and 2 months after implantation. Nuclei were stained with Hoechst 33342 (blue). Dashed lines are used to distinguish boundaries between L (lumen), G (graft), and T (surrounding tissues). Arrows indicate neovascularization on the outer surface of the grafts. Scale bar = 50μm.

3.3.4 Recruitment of SMCs and Vascular Wall Remodeling

Endothelialization provides vascular grafts with the antithrombotic property, which is necessary for a graft to stay patent. To obtain the desired mechanical properties, remodeling of the vascular wall relies on successful recruitment of SMCs. To investigate recruitment of SMCs to the grafts, cross-section immunostaining with primary antibodies against αSMA, an early SMC marker, and CNN1, an intermediate SMC marker, was performed.

At 2 weeks after implantation within the graft walls of both the heparin and heparin-SDF-1α groups, sparse cells that are αSMA positive but CNN1 negative were observed near the luminal surface of the grafts (Figure 3.5A-B). The marker expression of these cells suggests these are not mature SMCs. In addition to the region within the vascular grafts, many αSMA and CNN1 double positive cells were recruited to the tissue surrounding the grafts in both heparin and heparin-SDF-1α groups. The αSMA and CNN1 double positive cells around the heparin grafts were less organized, aligned in random orientation. In contrast, the double positive cells near heparin-SDF-1α graft were organized and aligned in the same direction, forming a fibrous tissue structure.

At 2 months after implantation, both the heparin and heparin-SDF-1α grafts had developed a neointimal formation. The only patent heparinized graft had developed a narrowed lumen and a thick neointima. Most cells in the neointima were found to be αSMA positive; only a small subset of these cells was also CNN1 positive (Figure 3.5A). In comparison, no apparent lumen narrowing was observed in patent heparin-SDF-1α grafts, and they had developed a thinner layer of neointima. The cells in neointima exhibited an organized and aligned structure. Moreover, they were positive for αSMA and CNN1, suggesting the cells had finished or in the process of differentiating into mature SMCs (Figure 3.5B). Cells in the tissue surrounding the heparinized graft remained as αSMA and CNN1 double positive. They were organized and aligned and had begun to form a fibrous tissue structure. The fibrous tissue surrounding the heparin-SDF-1α grafts were observed to be αSMA and CNN1 double positive. However, the number of cells that were positive for CNN1 was apparently less than 2-week heparin-SDF-1α grafts or the 2-month heparinized grafts.

3.3.5 Inflammatory Responses and Recruitment of Macrophages

In addition to ECs and SMCs, immune cells are expected to be recruited to the vascular grafts since the grafts are foreign materials and would surely trigger inflammatory responses. To investigate the type of immune cells recruited, cross-sections of the grafts were immunostained with primary antibodies against CD68, a pan-macrophage marker, CD163, an M2 macrophage marker, and CD11b, a monocyte marker. Overall, the inflammatory responses and cell recruitment to the grafts did not exhibit a big difference between heparin and heparin-SDF-1α groups, at either 2 weeks or 2 months after implantation. At 2 weeks, anti-inflammatory CD163 positive M2 macrophages were observed in the outer tissues surrounding the grafts (Figure 3.6), suggesting a “fixing” mechanism was initiated by the host to repair the wound.

Simultaneously, the pro-inflammatory “fighting” mechanism was also observed. CD68 positive pan-macrophages were observed within and directly adjacent to the grafts. Since M2 macrophages were only observed in the outer layer of surrounding tissues, it is reasonable to speculate that the macrophages residing within the grafts were the pro-inflammatory “fighting” M1 phenotype. In addition, CD11b positive monocytes were observed in the tissue directly adjacent to the grafts, marking the early stage of inflammatory responses. At 2 months after implantation, the distribution pattern of CD68 and CD163 positive cells remained the same as 2-week samples. However, the expression of CD11b disappeared in the cells adjacent to the grafts, suggesting the inflammatory responses had transitioned from the early to middle/late stage.

3.3.6 Calcification of Vascular Grafts

Calcification is one of the most catastrophic complications that could occur to biodegradable vascular grafts and jeopardize its long-term *in vivo* performance (71). To determine whether the implanted vascular grafts had triggered calcium deposition, Alizarin Red S staining was performed on the graft samples. Staining results showed that for up to 2 months, no calcification was observed in both heparin and heparin-SDF-1α groups (Figure 3.7).

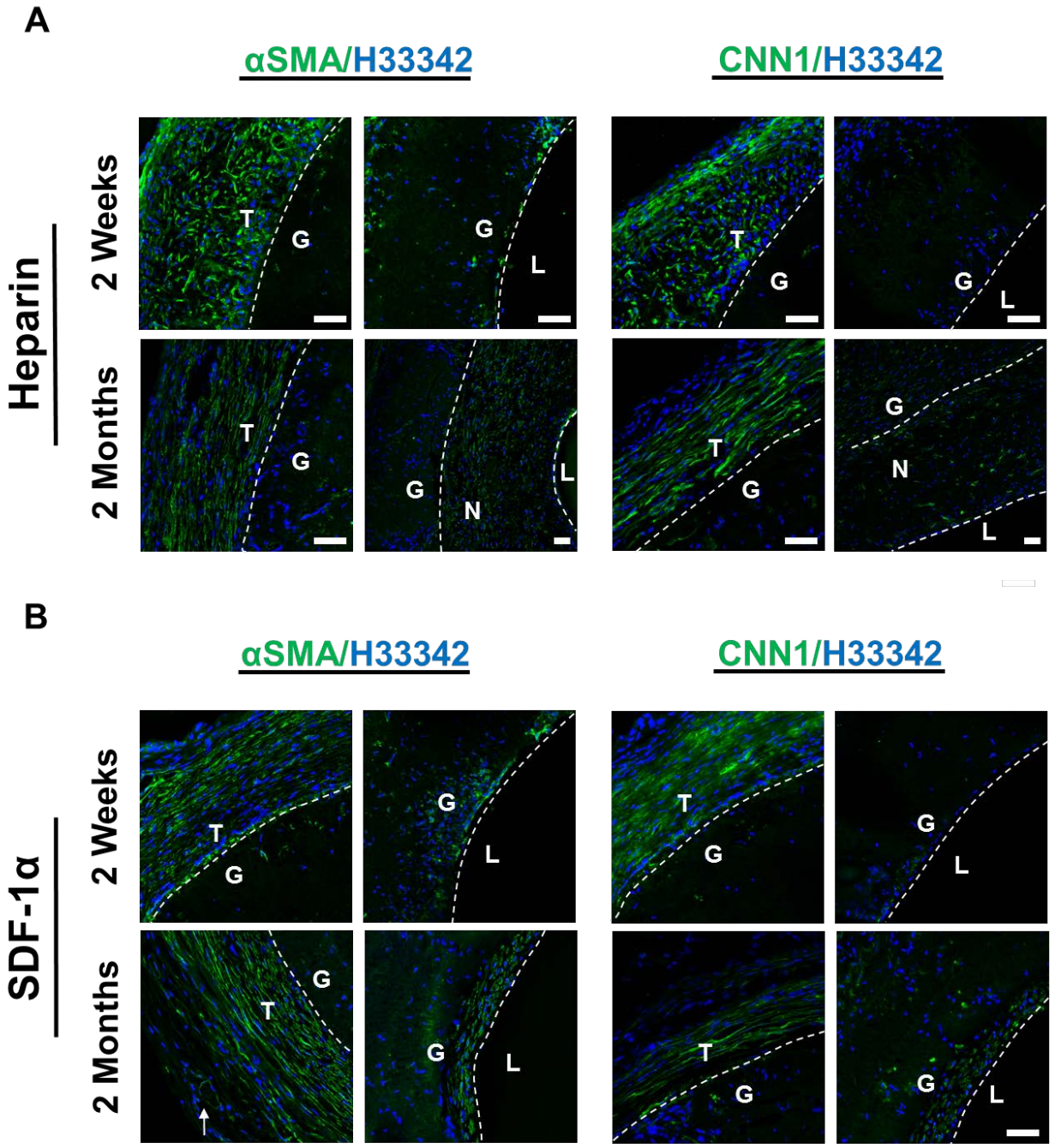

Figure 3.5 Identification and characterization of SMCs. Immunostaining for αSMA (green) and CNN1 (green) of (A) heparinized and (B) SDF-1α immobilized grafts at 2 weeks and 2 months after implantation. Nuclei were stained with Hoechst 33342 (blue). Dashed lines are used to distinguish boundaries between L (lumen), N (neointima), G (graft), and T (surrounding tissues). Arrow indicates neovascularization on the outer surface of the grafts. Scale bar = 50μm.

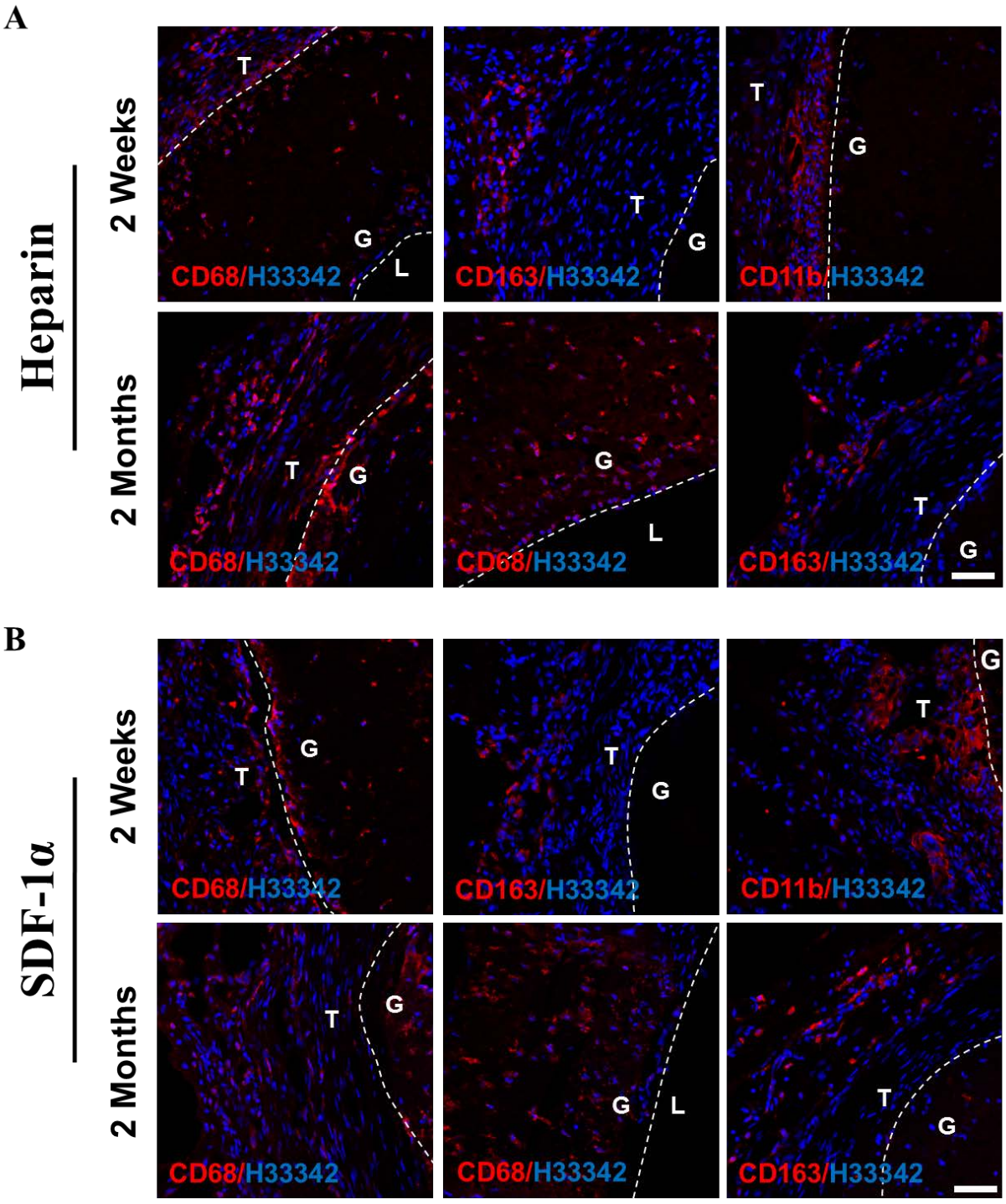

Figure 3.6 Inflammatory responses of vascular grafts. Immunostaining for CD68 (red), CD163 (red) and CD11b (red) of (A) heparinized and (B) SDF-1α immobilized grafts at 2 weeks and 2 months after implantation. Nuclei were stained with Hoechst 33342 (blue). Dashed lines are used to distinguish boundaries between L (lumen), G (graft), and T (surrounding tissues). Scale bar = 50μm.

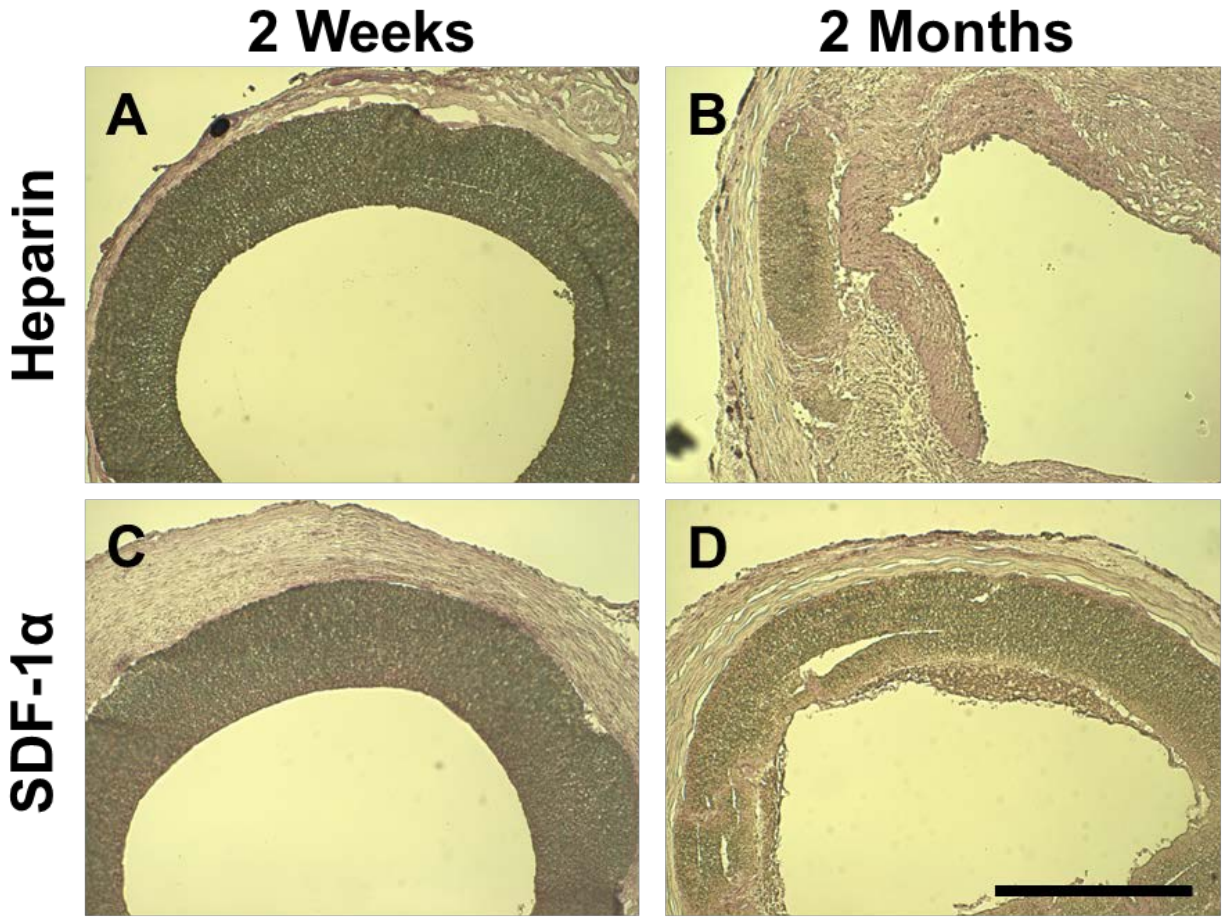

Figure 3.7 Calcification of vascular grafts. Alizarin Red S staining of vascular grafts at 2 weeks and 2 months after implantation for heparinized (A, B) and SDF-1α immobilized (C, D) groups. Scale bar = 0.5mm.

3.4 Discussion

Tissue engineering is a field that utilizes a combination of cells, materials, and engineering to improve or replace native tissues. A cell-free approach to tissue engineering is less common and relatively new. It requires the use of slow-degrading polymer and relies on the regenerative capability of the host. The previous chapter described the development of a cell-free small-diameter microfibrous vascular graft using PLCL and PDO. In this study, we characterized the mechanical properties and the *in vivo* biological performance of the vascular graft.

The mechanical characterization demonstrated that the PLCL/PDO blend grafts have an elastic modulus on the same order as the native artery. The PLCL component of the graft has enhanced the mechanical strength of the graft. The grafts were able to meet the most fundamental physical requirement, which is to withstand the suture force during anastomosis surgery and arterial pressure immediately upon implantation. *In vitro* hydrolytic degradation results showed that while the grafts lost only 10% of its mass after 4 weeks, its ultimate tensile strength dropped to 20% of its pre-degradation counterpart. However, under *in vivo* environment, in which the degradation and loss of mechanical strength are accelerated, the vascular grafts were able to stay in shape and provide structural support after 2 months of implantation. This suggests that both the cells infiltrated into the grafts and the tissue growing around the grafts compensated for the loss of mechanical strength.

In addition to providing mechanical and structural supports, an ideal cell-free vascular graft should be able to tap into the full regenerative potential of the host to promote endothelialization and remodeling of the vascular wall. Acute thrombosis is the major reason for failure in small-diameter vascular grafts. Although it can be temporarily suppressed by heparin, an anticoagulant that has anti-thrombogenic property, oral anticoagulant and antiplatelet therapies might still be necessary to maintain long-term patency. Endothelium produces anticoagulants such as heparin sulfate and hence provides a non-thrombogenic surface. Therefore, for a vascular graft to succeed, it is crucial to have a rapid endothelialization of the graft. SDF-1α is a chemokine that has been reported to attract EPCs and accelerate endothelialization of vascular grafts (18). In addition, heparin has been reported to bind and stabilize SDF-1α without interfering with its chemotactic activities (72-75). (More details on structure and function of SDF-1α is discussed in next chapter) The *in vitro* results reported herein showed that immobilized SDF-1α on heparinized grafts is more stable and has slower *in vitro* release than passively absorbed SDF-1α under static conditions.

The results of *in vivo* studies reported herein showed that the vascular grafts were able to recruit ECs and EPCs within 2 weeks. However, endothelialization was incomplete, and patches of coverage of the luminal surface by ECs and EPCs were observed throughout the grafts. Thrombus formation was observed in all occluded grafts at 2 weeks after implantation, indicating the significance of heparinization of vascular grafts at an early stage. 2 months after implantation, 5 of 6 heparinized grafts were occluded, and obvious narrowing and extensive neointimal formation was observed in

the patent heparinized graft. In contrast, 1 of 5 heparin-SDF-1α grafts was occluded, and no obvious neointimal hyperplasia was observed in the patent heparin-SDF-1α grafts. Although the cross-section immunofluorescent staining of the patent grafts showed no apparent difference in EC coverage between the heparin and heparin- SDF-1α groups, the difference in patency suggests it is most likely that occluded heparinized grafts had incomplete EC coverage. There are two main mechanisms whereby vascular grafts recruit ECs. The first mechanism is the transanastomotic migration of ECs from the adjoining arteries. The second mechanism is adhering and differentiation of EPCs recruited from the bloodstream. SDF-1α immobilized on the vascular grafts is expected to recruit more EPCs from the bloodstream; it can further promote endothelialization of the grafts by inducing proliferation and differentiation of adhered ECs (76, 77). As a result, heparin-SDF-1α grafts had an accelerated endothelialization and hence better long-term patency compared to heparinized grafts. This indicates the necessities of a rapid endothelialization and consequential non-thrombogenic surface. In this study, the effect of SDF-1α was investigated using a healthy rat model, which has a strong regenerative ability. Their ECs have greater capacity to migrate and cover the luminal surface of the vascular grafts than those of humans, especially aged human with diseased blood vessels (78, 79). The performance of heparin-SDF-1α grafts in large animals is yet to be investigated. It is expected that SDF-1α will have a more pronounced effect in large animals and possibly be an essential component in a diseased model.

Other than endothelialization, another important criterion for a successful vascular graft is remodeling of the vascular wall as SMCs contribute to necessary elasticity and mechanical strength of the vascular grafts. The results reported herein showed that the heparin-SDF-1α grafts were able to recruit SMCs, demonstrating that the host possesses the potential to carry out vascular regeneration with endogenous cells without the aid of a cell-seeding graft. The advantage of cell-seeding grafts is that they can enhance biocompatibility and anti-thrombogenic property, which might lead to better long-term patency. However, the approach faces various challenges such as cell characterization, survival in the grafts during preparation and surgery, and attachment under native flow condition.

When a fast-degrading foreign material is exposed to a host, it is expected to induce an immune response; the PLCL/PDO blend graft was not an exception. It was observed that M1 “fighting” macrophages were recruited into the grafts and M2 “repairing” macrophages were recruited to the tissue around the grafts. Recruitment of macrophages when using a foreign vascular graft is more or less inevitable. However, it can be harmful when the accumulation of macrophages in the blood vessel can induce inflammation-dependent calcification and influence propagation of the calcification (80-83). Calcification in the vascular grafts has a detrimental effect on its long-term biological performance. A recent study with 40 PTFE vascular grafts harvested from human patients suggests that calcification may play a role in eventual graft failure. Calcification was observed in neointima and within the graft itself, and the degree and extent of calcification were associated with the duration of graft implantation (84). In this study, no calcification was observed at 2 months after implantation. However, long-term

studies would be required to fully assess the calcification of the vascular grafts presented herein.

In this study, we characterized the mechanical properties and *in vivo* performance of previously developed cell-free small-diameter PLCL/PDO blend vascular grafts. We also investigated the combined effect of chemokine SDF-1α and vascular grafts on endothelialization and SMCs recruitment. A previous study by Yu et al. has also investigated the effect of heparin-SDF-1α vascular grafts on the recruitment of ECs and SMCs (18). In their study, the vascular grafts were fabricated using a PLLA and PCL polymer blend, and the effect of SDF-1α on the recruitment of ECs and SMCs was more pronounced than it was observed in this study. However, in Yu's study, the heparinized grafts had limited cell infiltration, and the cell recruitment relied heavily on the presence of chemokine SDF-1α. In contrast, PLCL/PDO blend grafts used herein were able to recruit a decent amount of ECs and SMCs without SDF-1α; this factor somewhat diminished the difference in cell recruitment caused by SDF-1α. Our study demonstrated the important roles played by both biomaterial and medicine in tissue engineering. More research needs to be done to acquire an optimal combination that maximizes their utilities.

There are some limitations in this study that need to be addressed in future work. For instance, the small animal model used in this study cannot fully recapitulate the response in human beings (78). Moreover, our *in vivo* study was terminated at 2 months; the long-term biological performance is yet to be determined. To fully assess the potential of heparin-SDF-1α PLCL/PDO vascular grafts, long-term studies using large animal models need to be investigated.

Chapter 4: *C*-terminal Modification of Stromal Cell-derived Factor-1α Significantly Affects its Chemotactic Activity

4.1 Introduction

4.1.1 Structure and Function of Stromal Cell-Derived Factor-1

Chemokines are chemotactic cytokines that have the ability to direct cell migration (85). All reported human chemokines have a three-dimensional structure composed of a three-stranded β-sheet followed by an α-helix. The structure of human chemokines is stabilized by two disulfide bonds formed between conserved cysteine residues (86). Depending on the spacing of the first two cysteine residues, the chemokines can be divided into two major families: the CXC- and the CC- chemokines. Chemokines transmit signals to selective cells by binding to chemokine receptors that are found on the cell membrane surface of their target cells. Usually, one chemokine binds to multiple receptors, and the same receptor can bind to multiple chemokines. It was originally thought that chemokine CXCL12 (or SDF-1) was limited to binding only to CXCR4 (CXC chemokine receptor 4) (87-94). Recently, however, it was reported to interact with CXCR7 as well (95); this interaction is not yet well understood.

SDF-1 has two main isoforms, SDF-1α and SDF-1β, by alternate splicing (96). SDF-1α has approximately 70 amino acids with first eight amino acids being the active binding site. SDF-1α is the predominant isoform found in all organs, but it has weaker resistance against blood-dependent proteases such as MMP-2 compared to isoform SDF-1β (97).

SDF-1 is able to attract a variety of cell types that express CXCR4 receptors including muscle cell lines, ECs, leucocytes, and progenitor cells (98-100). SDF-1 has been reported to regulate various physiological processes including embryonic development, organ homeostasis, and angiogenesis (101, 102). In particular, the angiogenic properties of SDF-1 make it a promising candidate for the therapeutic treatment of tissue ischemia.

4.1.2 Sulfhydryl-Reactive Crosslinker Chemistry

Forming a stable covalent bond between a protein and another (bio) molecule is a powerful technique used to modify protein function (103-106). Aside from amine-based reactions, the most common crosslinkers and protein modifications involve using a sulfhydryl or thiol group (-SH) (107). Thiol groups are very useful for protein conjugations or modifications. They are not as abundant as primary amines, making crosslinking via thiol groups more selective and precise (108, 109). In addition, reactions through thiol groups, in general, do not significantly change the protein structure thus minimizing the risk of impairing the functions of modified protein (107).

The amino acid cysteine is an excellent tool for protein bio-conjugation. In addition to being the only amino acid with a free thiol group in its side chain, it is very

rare to find free cysteine residue on the protein surface. These two properties make a thiol-reactive crosslinking on cysteine very specific (107).

Proteins that carry a free thiol group are able to form disulfide bonds (-S-S-) with itself as the basis of native tertiary or quaternary protein structure (107). It could also react with thiol-reactive compounds such as maleimides ($H_2C_2(CO)_2NH$). Under a mild basic condition, the thiol group on cysteine will be deprotonated to become a thiolate nucleophile ($-S^-$). It will react with soft electrophiles such as maleimides and form a stable irreversible carbon-sulfur bond (107, 110). A schematic of such a maleimide reaction is shown in Figure 4.1.

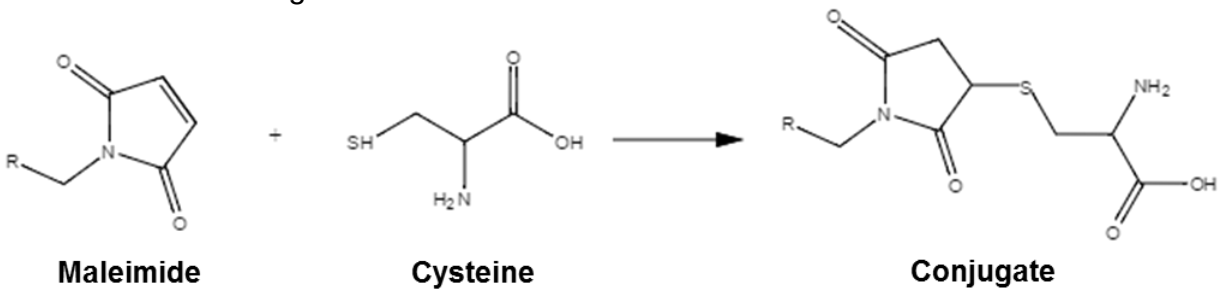

Figure 4.1 Maleimide reaction scheme for chemical conjugation to the sulfhydryl group on cysteine.

4.1.3 Heparin-SDF-1α Interaction

SDF-1α was originally shown to possess high-binding affinity to heparin through a proposed mechanism of non-specific electrostatic interactions (111). However, this binding was later shown to be specific. To better study this SDF-1α-heparin interaction, researchers used point mutagenesis to create a modified SDF-1α that has three point mutations on its first β-strand. It was shown that although this modified SDF-1α maintains its global negatively charged structure and *in vitro* functional properties, its affinity to heparin is significantly decreased (72). Using a SDF-1α/heparin complex model and electrostatic potential map, researchers later suggested heparin primarily interacted with the basic amino acid residues Lys^1, Lys^{24}, His^{25}, Lys^{27}, Arg^{41}, and Lys^{43} and secondarily with Asn^{46} and Gln^{48} (74). Moreover, it was shown binding to heparin stabilizes and protects SDF-1α from enzymatic degrading by protease CD26/dipeptidyl peptidase (75).

4.2 Materials and Methods

4.2.1 WT- and Cys-SDF-1α Expression, Isolation, Refolding, and Purification

WT- and Cys-SDF-1α cloning and expression vector construction

The cloning of 2AT-WT-SDF-1α and 2AT-Cys-SDF-1α plasmid was performed by QB3 MacroLab at University of California, Berkeley. WT- and Cys-SDF-1α gene inserts were amplified using Phusion polymerase (New England BioLabs Inc., Ipswich, MA) with WT-SDF-1α and Cys-SDF-1α forward and reverse primers. Vector 2AT (QB3 MacroLab, Berkeley, CA) was digested using restriction enzyme EcoRV (New England BioLabs, Inc.). The resulting vector backbone and amplified WT- and Cys-SDF-1α gene inserts were ligated using a Gibson assembly. The resulting 2AT-WT-SDF-1α and 2AT-Cys-SDF-1α plasmids were transformed into XL1-Blue competent cells. Amplified plasmids were sequenced with T7 forward and reverse primers to verify the insertion of WT- and Cys-SDF-1α. Sequences of all primers used and SDF-1αs are illustrated in Table 4.1.

WT- and Cys-SDF-1α Forward	5'-TTTAAGAAGGAGATATAGATCATGAAACCAGTTTCGCTGTCCTACCG-3'
WT-SDF-1α Reverse	5'-TTATGGAGTTGGGATCTTATTATTTATTCAGCGCTTTTTCCAGATATTCC-3'
Cys-SDF-1α Reverse	5'-TTATGGAGTTGGGATCTTATTAACATTTATTCAGCGCTTTTTCCAGATATTCC-3
T7 Forward	5'-TAATACGACTCACTATAGGG-3'
T7 Reverse	5'-GCTAGTTATTGCTCAGCGG-3'
WT-SDF-1α gene	ATGAAACCAGTTTCGCTGTCCTACCGCTGTCCATGCCGTTTCTTCGAGAGCCATGTCGCGCGTGCGAATGTTAAACATCTCAAAATTTTGAATACTCCGAACTGTGCACTCCAGATCGTGGCACGTTTGAAAAACAACAACCGCCAAGTGTGCATTGATCCTAAACTGAAATGGATCCAGGAATATCTGGAAAAAGCGCTGAATAAATAA
Cys-SDF-1α gene	ATGAAACCAGTTTCGCTGTCCTACCGCTGTCCATGCCGTTTCTTCGAGAGCCATGTCGCGCGTGCGAATGTTAAACATCTCAAAATTTTGAATACTCCGAACTGTGCACTCCAGATCGTGGCACGTTTGAAAAACAACAACCGCCAAGTGTGCATTGATCCTAAACTGAAATGGATCCAGGAATATCTGGAAAAAGCGCTGAATAAATGTTAA

Table 4.1 WT- and Cys-SDF-1α sequences and primers for molecular cloning.

Inducible Expression of WT- and Cys-SDF-1α

To express WT- and Cys-SDF-1α, Rosetta 2(DE3)pLysS competent cells were transformed with 2AT-WT-SDF-1α and 2AT-Cys-SDF-1α plasmids, respectively, and subsequently cultured on agar plates containing carbenicillin (100μg/ml). A single

colony was picked and incubated overnight in 25 mL of 2YT media with carbenicillin (100µg/ml) on a shaker at 37^{o}C. One liter of 2YT media with carbenicillin (100µg/ml) was inoculated with 10 mL of the overnight starter culture and incubated with shaking at 37^{o}C. When O.D.600 of the culture reached 0.6, IPTG was added to achieve a final concentration of 1mM to induce protein expression. Induced cells were allowed to grow for 4 hours and subsequently harvested by centrifuging at 4,000 rpm at 4^{o}C for 15 minutes. The cell pellets were re-suspended in 20 mL of PBS with 10% glycerol and homogenized. The cell lysate was centrifuged at 15,000 rpm for 30 minutes at 4^{o}C; WT- and Cys-SDF-1α were found in the inclusion bodies.

Isolation and Refolding of WT- and Cys-SDF-1α

WT- and Cys-SDF-1α were extracted and isolated following previously published protocol (73). In short, inclusion bodies were washed 3 times with buffer A (100mM Tris-HCl, 5mM EDTA, 5mM dithiothreitol, 2M urea, 2% Triton X-100, pH 8.0) and once with buffer B (100mM Tris-HCl, 5mM EDTA, 5mM dithiothreitol, pH8.0). During each wash, the supernatant was discarded, and inclusion bodies were resuspended in the buffer thoroughly and sonicated for 5 minutes. Resuspended samples were subsequently centrifuged at 13,000 rpm at 4^{o}C for 20 minutes. After the last wash with buffer B, inclusion body pellet was solubilized in 6M guanidine-HCl (5mL guanidine-HCl per 1L bacterial culture), and diluted 1:100 into refolding buffer (100mM Tris-HCl, 5mM EDTA, 0.2mM oxidized glutathione, 1mM reduced glutathione, pH 8.0) and stirred at 4^{o}C overnight.

WT- and Cys-SDF-1α Purification

Traditionally, refolded SDF-1α purification would employ the use of size exclusion chromatography and reverse phase HPLC. However, due to lack of access to the aforementioned methods, in this study two different molecular weight cutoff- (MWCO) sized protein concentrators were used to desalt and purify SDF-1αs. Refolded WT- and Cys-SDF-1α were filtered through a 0.22µm filter system to remove cell debris and other large insoluble compounds. Protein samples were subsequently concentrated with 5K MWCO UF centrifugal concentrators (Corning). This concentration step simultaneously removes contaminants that are smaller than 5K MWCO in average size. Concentrated protein samples were diluted in storage buffer (10mM HEPES, 150mM NaCl, pH 7.9) and concentrated again, using the same 5K MWCO concentrators. This dilution followed by a concentration step was repeated a few times using storage buffer to remove refolding buffer at the greatest extent. Lastly, the protein samples were filtered through 30K MWCO centrifugal concentrators (EMD Millipore) to remove contaminant proteins bigger than 30K MWCO in average size. SDS-PAGE was performed on final purified protein followed by Simply Blue staining (Thermo Fisher) and Western blotting procedures to determine the protein purity. The commercially available SDF-1α ELISA kit (R&D Systems) was used to quantify the SDF-1α concentration.

4.2.2 Jurkat Cell Culture and Chemotaxis

Jurkat cells were purchased from UC Berkeley's Cell Culture Facility (Berkeley, CA). The cells were grown in RPMI Medium 1640 (Invitrogen) containing 10% FBS and 1% penicillin-streptomycin, and kept at a density between 10^5 to 10^6 cells/mL.

Migration of Jurkat cells was performed using HTS Transwell-96 Permeable Support (Corning) with a 5.0μm membrane pore size. The bottom chambers of HTS Transwell were filled with 140 μL of migration medium (RPMI 1640, 1% FBS) containing chemo-attractants at different concentrations. The HTS Transwell inserts were placed into the wells, and 100 μL cell suspension containing 10^5 cells was added to each top chamber. The cells were allowed to migrate for 4 hours at 37^oC in a CO_2 incubator. Chemotactic activities of commercial SDF-1α (PeproTech), WT- and Cys-SDF-1α at different concentrations (1, 10, and 100 ng/mL) were tested. Migration medium with no chemo-attractant added was served as negative control. Migration medium containing a higher concentration of FBS (10%) was used as a positive control.

Following cell migration, the HTS Transwell insert was removed. The medium in bottom chambers containing migrated cells from top chambers was collected, and migrated cells were counted using hemocytometer.

4.2.3 Hydrogel Encapsulation of SDF-1αs

A collagen- and heparin-containing hyaluronic acid based hydrogel kit was commercially purchased (Hystem-HP, BioTime). In order to produce a hydrogel with optimal stiffness, crosslinker was used at a concentration four times higher than the manufacturer's recommendation. To encapsulate the SDF-1αs, commercial and Cys-SDF-1α in PBS was used to reconstitute the crosslinker and mixed with hydrogel backbone solution to achieve a final SDF-1α concentration of approximately 25ng/mL. Mixed hydrogel solution was allowed to crosslink for 30 minutes before implantation. A hydrogel containing no SDF-1α was used as a negative control.

4.2.4 *In Vivo* Subcutaneous Implantation and Explantation

The animal protocol was developed and approved before surgery. All procedures were approved by the Institutional Review Board Service and the Institutional Animal Care and Use Committee at the University of California, Berkeley. Approximately 12-week-old male TIE-2-GFP transgenic mice were purchased from The Jackson Laboratory. The mice were anesthetized with 2.0% isoflurane in 70% nitrous oxide and 30% oxygen. Abdominal skin was dissected. 50 μL of SDF-1αs (commercial and Cys-SDF-1α) encapsulated Hystem-HP hydrogels were placed in between the fascia and muscle. The wound was sutured with a 4-0 needle. At the time of explantation after 2 weeks *in vivo*, the animals were euthanized, and the hydrogels were explanted.

4.2.5 Histological Analysis

The explanted hydrogels were fixed with 4% PFA for 2 hours and subsequently kept overnight in an OCT compound at 4^{o}C. The OCT compound infiltrated hydrogels were frozen and sectioned into 20μm-thick slices using a cryostat. Slides were incubated with Hoechst 33342 for 10 minutes, followed by fluorescent microscopy.

4.2.6 Statistical Analysis

Student's t-test was performed to detect whether a significant difference exists between two sample groups. For multiple sample comparisons, ANOVA was used first to detect whether or not there was a significant difference among the groups, and Holm's t-test was subsequently performed on all possible pairs to isolate the different sample. A p-value of 0.05 or less was considered to have a significant difference.

4.3 Results

4.3.1 Characterization of Purity of SDF-1αs

Molecular cloning of DNA plasmids for WT-SDF-1α and Cys-SDF-1α was outsourced to QB3 MacroLab at the University of California, Berkeley. Protein expression, isolation, refolding, and purification were done in-house. In order to achieve high protein purity for subsequent studies and analysis, protein purification would usually involve utilizing chromatography based on size, charge, and/or hydrophobicity. Unfortunately, due to timeframe limitations and lack of access to required facilities, the purification process in this study was compromised. Two different MWCO sized protein concentrators were used to desalt and purify SDF-1αs. To compare the purities of in-house isolated and refolded WT- and Cys-SDF-1α, commercially available SDF-1α was purchased and used in this study as a positive control.

To determine the purity of isolated WT- and Cys-SDF-1α, SDS-PAGE was performed on commercial SDF-1α and purified WT- and Cys-SDF-1α in their reduced and non-reduced form followed by total protein staining and Western blotting. Total protein staining of SDF-1αs showed that the commercial SDF-1α had a clear band for both reduced and non-reduced form (Figure 4.2A). Interestingly, SDF-1α showed a "mobility shift" between the reduced and non-reduced form. Under the reduced condition, SDF-1α showed a band at around 10kDa, which is the molecular weight of the commercial SDF-1α. When run at the non-reduced condition, the band was retarded to around 15kDa. When in-house isolated WT- and Cys-SDF-1α were run under reduced condition, both samples showed one strong band at around 10kDa; this suggests that the use of two MWCO sized protein concentrators effectively removed the majority of the out-of-range (larger than 30kDa and smaller than 5kDa) protein contaminants. Unlike commercial SDF-1α, however, both WT- and Cys-SDF-1α had more than one protein bands when they were run under the non-reduced condition. WT-SDF-1α had two weak bands: one band was located at around 15 kDa corresponding to the "shifted" SDF-1α, and the second one was located at around 10kDa. Cys-SDF-1α also had two bands at the same location as WT-SDF-1α, but the intensity of the band at 15kDa was much stronger than the band at 10kDa. The weak bands at 10kDa of the non-reduced protein suggest that it is likely that there were contaminant proteins in the samples. Because the purification process used in this study is based exclusively on protein size, it is not surprising to have contaminant protein of similar molecular weight.

Simply Blue staining showed the presence of protein in the sample. However, it was unable to identify the protein presented to be SDF-1α. Therefore, the Western blotting was performed on the protein samples with an antibody against SDF-1α. Results showed WT- and Cys-SDF-1α under reduced condition both had one band at around 10kDa, confirming the presence of SDF-1αs in the samples (Figure 4.2B). Under the non-reduced condition, Cys-SDF-1α had one shifted weak band at around 15 kDa. WT-SDF-1α under non-reduced condition showed three bands, one band at around 10kDa and one band at around 15kDa, similar to the results found in the total protein staining. There was surprisingly a third band in between. A possible explanation for this

is that during the concentrating process, WT-SDF-1α was fragmented into shorter pieces that are still able to be recognized by the antibody. SDF-1α quantification by ELISA showed isolated WT-SDF-1α had a much higher concentration than its cysteine modified form. Therefore, it is possible that Cys-SDF-1α was also fragmented, but the concentration of fragmented pieces was below the detection limit.

To further confirm the presence of WT- and Cys-SDF-1α, protein samples were sent to Proteomics/Mass Spectrometry Laboratory at the University of California, Berkeley for proteomic analysis. The results (not shown) indicated that the SDF-1α was the most abundant protein in the samples, yet there were various E.coli proteins presented in the samples as well.

The combination of total protein staining, Western blotting, and proteomic analysis proved that it is possible to express and isolate WT- and Cys-SDF-1α. The purity of the protein, however, could be further improved by introducing chromatography steps.

4.3.2 *In Vitro* Chemotactic Activity of SDF-1αs

Although the characterization of isolated proteins presented herein confirmed the presence of WT- and Cys-SDF-1α, no conclusion about bioactivities of SDF-1αs from these assays can be drawn. To determine the bioactivities of WT- and Cys-SDF-1α, *in vitro* chemotaxis assay using Jurkat cells, a common and easy way to test the bioactivity of SDF-1α, was performed. Using a transwell chamber designed for chemotaxis assay, Jurkat cells were allowed to migrate for 4 hours while being exposed to commercial, WT- or Cys-SDF-1α at different concentrations (1, 10, and 100 ng/mL). Migration medium which was basal medium containing 1% FBS was used as a negative control. Basal medium containing 10% FBS was used as a positive reaction control.

Results showed that Jurkat cells had a migration efficiency of 1.67 ± 1% in the negative control which contained 1% FBS (Figure 4.3). In the positive control, which contained 10% FBS, Jurkat cells migrated at an efficiency of 6.22 ± 1.26%, 3 folds higher than the negative control. This difference indicates that the Jurkat cells respond to chemo-attractant stimuli and were able to migrate with the assay set-up. When the concentration of SDF-1αs was as low as 1ng/mL, cell migration induced by commercial SDF-1α and WT-SDF-1α were comparable, at 4.33±2.5% and 5.44±1.89%, respectively. At the same low concentration, Cys-SDF-1α resulted in migration efficiency of 15.22±2.52%, 3 folds higher than commercial and WT-SDF-1α. This difference is statistically significant, with $p < 0.01$. When the concentration of SDF-1αs was increased to a moderate concentration of 10ng/mL, commercial and WT-SDF-1α samples showed similar migration efficiencies of 10.22±4.04% and 11.78±5.30%, respectively, with no significant difference. Cys-SDF-1α showed a significantly higher migration efficiency of Jurkat cells at 29.11±8.10%, which was still approximately 3 folds higher than commercial and WT-SDF-1α. When the concentration of SDF-1αs was further increased to a high concentration of 100ng/mL, commercial SDF-1α caused the Jurkat cells to migrate at 48.22±18.28% efficiency. WT-SDF-1α samples showed a slightly

lower efficiency of 33.89±20.1%, which was lower than commercial SDF-1α yet still higher than WT-SDF-1α at a moderate concentration. Surprisingly, Cys-SDF-1α caused a low cell migration efficiency of 4.44±2.76%, which was just slightly higher than the negative control.

Within the range of the concentration tested (1~100ng/mL), commercial SDF-1α exhibited a positive correlation between chemo-attractant concentration and migration efficiency. WT-SDF-1α exhibited a similar trend with comparable activity at low concentrations but lower activity at higher concentrations. Cys-SDF-1α, on the other hand, exhibited a biphasic correlation; it had high activity at intermediate concentrations, and its activity dropped drastically at lower or higher concentrations. Since WT-SDF-1α was expressed, isolated, refolded, and quantified using the same system, the different pattern between WT-SDF-1α and Cys-SDF-1α eliminated the possibility that the biphasic pattern was induced by contaminant E.coli proteins.

4.3.3 *In Vivo* Functional Performance of SDF-1αs

In vitro chemotaxis assay has demonstrated that refolded Cys-SDF-1α is biologically active and behaves differently compared to commercial SDF-1α. To determine whether Cys-SDF-1α also performs differently *in vivo*, a transgenic TIE-2-GFP mouse model was used. A hyaluronic acid based hydrogel containing collagen and heparin was used to encapsulate commercial SDF-1α and in-house isolated Cys-SDF-1α. SDF-1αs encapsulated hydrogels were subcutaneously implanted into 12-week-old male TIE-2-GFP transgenic mice. 2 weeks following implantation, hydrogel samples were explanted and imaged with a fluorescent microscope. At 2 weeks after implantation, there were limited cells infiltrated into the hydrogel; therefore TIE-2 expression in the surrounding tissue was examined. A blank hydrogel containing no SDF-1α was used as a negative control. Figure 4.4A shows that within the surrounding tissue, a small number of cells were TIE-2 positive, potentially recruited by the heparin component of the hydrogel as heparin has been reported to promote angiogenesis (112, 113). In comparison, both commercial SDF-1α and Cys-SDF-1α have recruited more TIE-2 positive cells (Figure 4.4B-C); however, no obvious difference was observed between commercial SDF-1α and Cys-SDF-1α samples at the concentration of 25ng/mL.

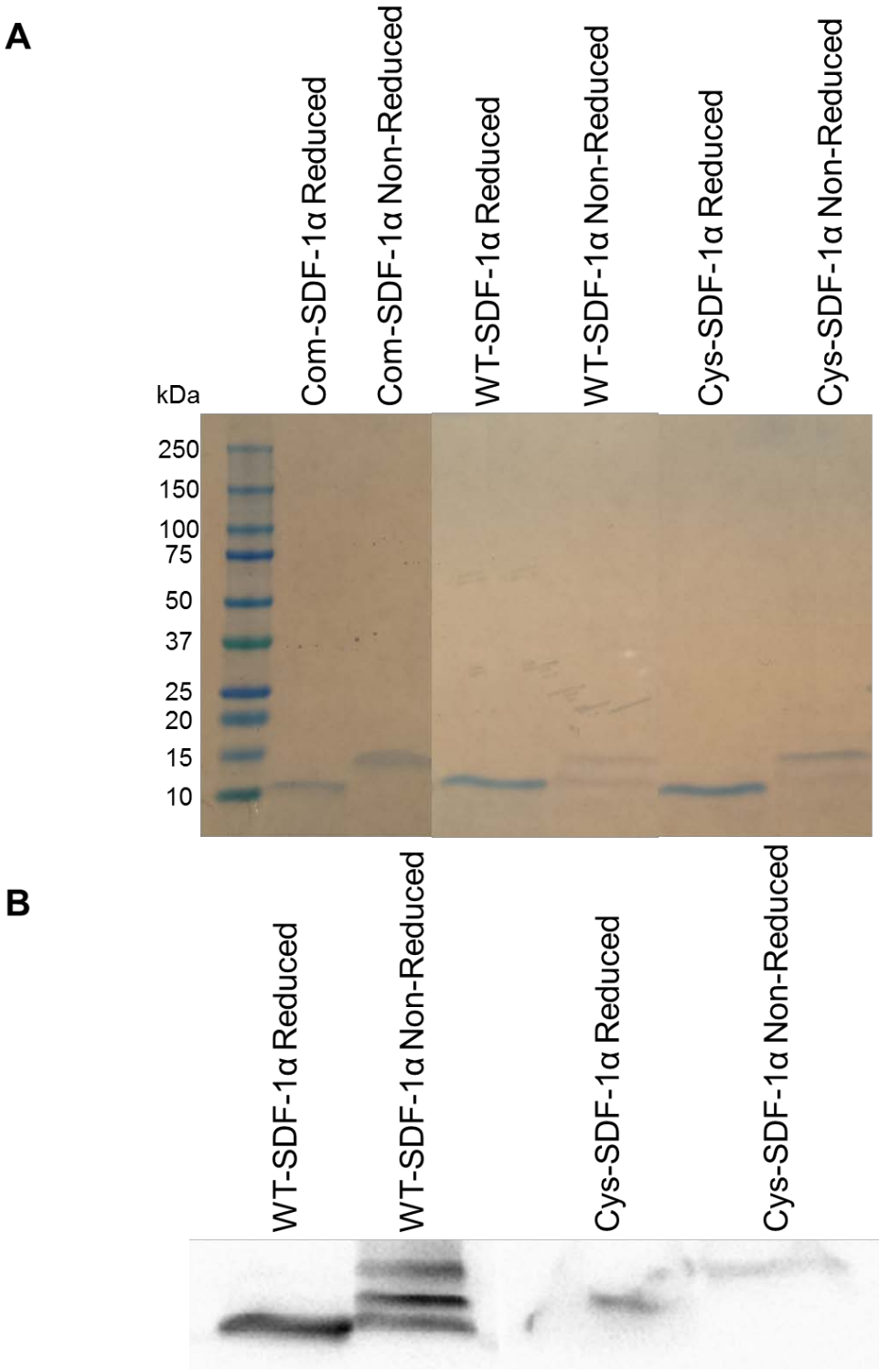

Figure 4.2 Characterization of expressed SDF-1αs. (A) Total protein staining of commercial SDF-1α, WT-SDF-1α and cys-SDF-1α in reduced and non-reduced condition. (B) Western blot of WT-SDF-1α and cys-SDF-1α in reduced and non-reduced conditions.

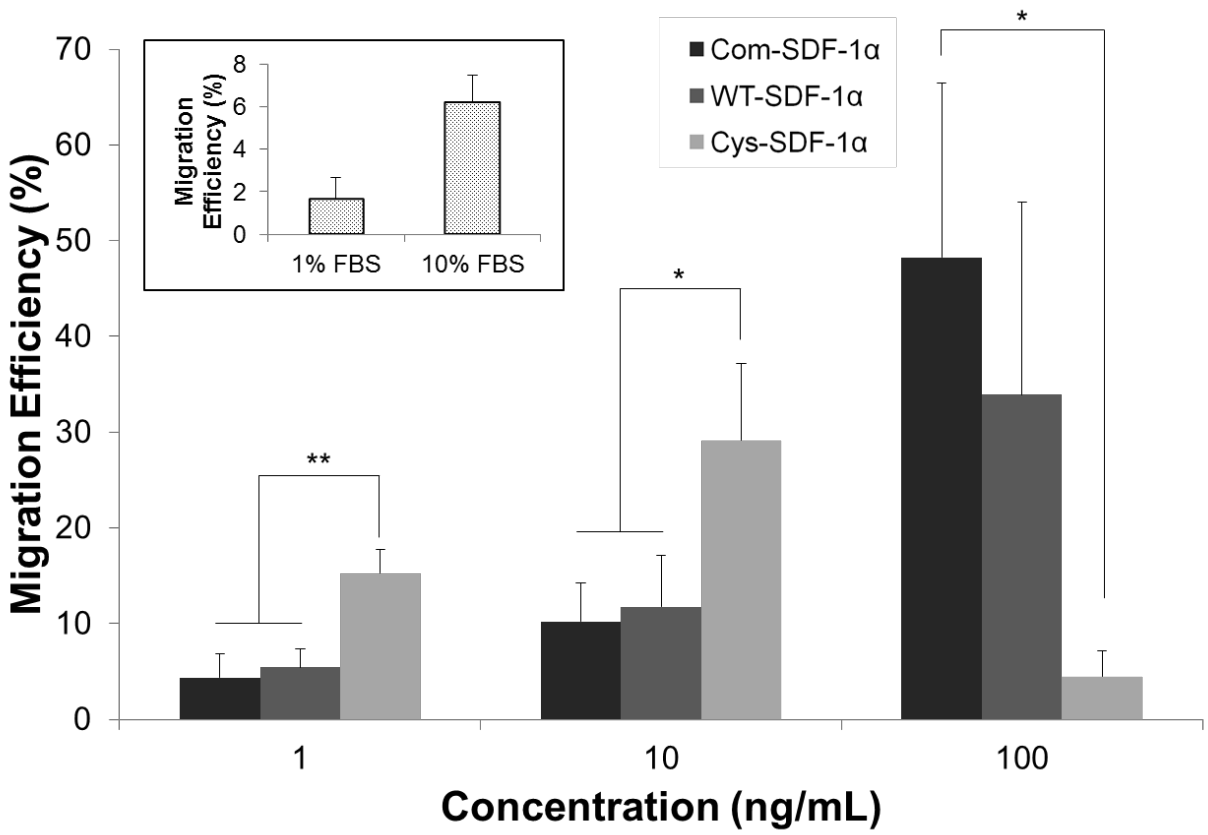

Figure 4.3 Chemotactic activities of SDF-1αs. Biological activities of commercial SDF-1α, WT-SDF-1α, and Cys-SDF-1α at varying concentration on the migration of Jurkat cells. Activities of 1% and 10% FBS were used as controls. * $p<0.05$, ** $p<0.01$, (n=3).

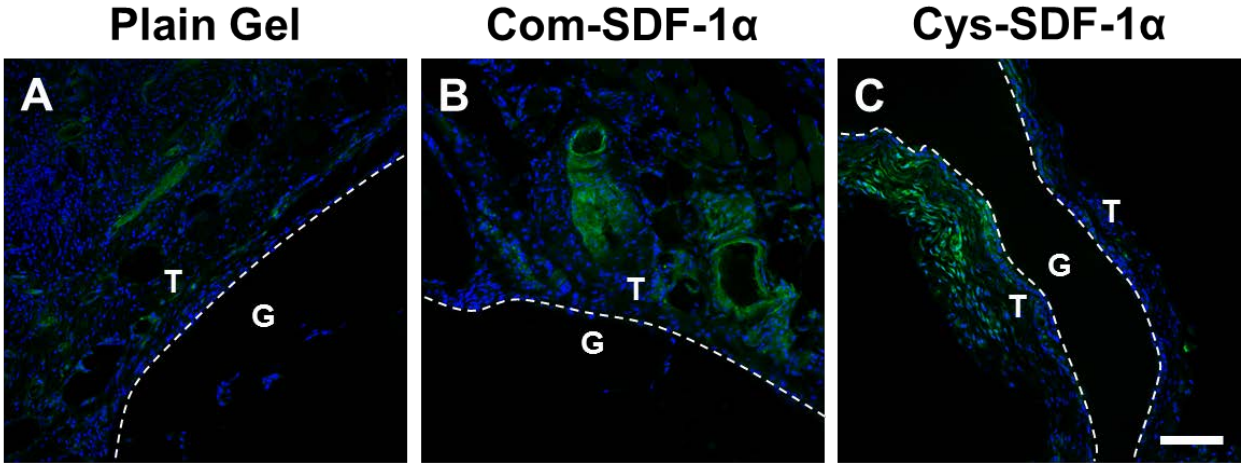

Figure 4.4 *In vivo* performance of SDF-1αs. Expression of TIE-2-GFP 2 weeks after subcutaneous implantation for (A) plain hydrogel, and hydrogel containing (B) commercial SDF-1α and (C) Cys-SDF-1α at a concentration of 25ng/mL. Nuclei were stained with Hoechst 33342 (blue). Dashed lines are used to distinguish boundaries between G (hydrogel) and T (surrounding tissues). Scale Bar = 100μm.

4.4 Discussion

SDF-1α is a chemokine that attracts a variety of CXCR4 and CXCR7 positive cells. This includes endothelial and muscle cells, which are essential for blood vessel formation. This property of SDF-1α makes it a promising candidate to be therapeutically used to promote angiogenesis. In addition, heparin, an anticoagulant commonly used in vascular surgeries, can bind to and stabilize SDF-1α. This suggests SDF-1α can potentially be used on its own in an injectable form to treat tissue ischemia or in combination with heparin-conjugated vascular grafts to accelerate *in situ* vascular regeneration. However, SDF-1α is very tiny in size (~10kDa), which leads to a fast diffusion. Moreover, the active site of SDF-1α is cleavable by proteases, dipeptidyl peptidase IV/CD26 and matrix metalloproteinase-2 for instance, which causes it to degrade rapidly in *in vivo* environment (114). As a result, it is very likely that majority of the SDF-1α is cleared from the *in vivo* system before it has an opportunity to induce angiogenesis.

To resolve the issue of fast clearance of SDF-1α, it would be beneficial to find a way to prolong the lingering of SDF-1α at targeted sites. For instance, conjugating multiple SDF-1α monomers to a single multi-armed PEG backbone would increase the size of chemokine, thus delaying its diffusion. SDF-1α monomers could also be anchored to targeted sites by directly conjugating to biomaterials such as microparticles or vascular grafts. One of the most common methods to perform chemical conjugation involves utilizing the thiol group on amino acid cysteine. Thiol is not as abundant as primary amines, and free cysteine is rarely found in protein. As a result, conjugation created with thiol chemistry would be relatively selective and precise.

As aforementioned, free cysteine is rarely found in protein, and SDF-1α is not an exception. Therefore, SDF-1α was engineered by introducing a free cysteine. Since the active site of SDF-1α is at its *N*-terminus, we, therefore, attached the cysteine residue to its *C*-terminus. In this study, we expressed, isolated, and purified the engineered Cys-SDF-1α and unmodified WT-SDF-1α. The *in vitro* biological activities of both WT- and Cys-SDF-1α were tested and then compared to commercially purchased SDF-1α. Results of *in vitro* chemotaxis assay showed that within the tested concentration range (1~100ng/mL), Cys-SDF-1α exhibits a biphasic pattern that is significantly different from the commercially purchased SDF-1α and WT-SDF-1α, which was expressed and isolated the same way as Cys-SDF-1α. Our results indicated that over the tested concentration range, for both commercial and WT-SDF-1α, a positive correlation between its concentration and chemotactic activity exists. However, Cys-SDF-1α exhibits a biphasic correlation where the highest biological activity was observed at an intermediate concentration (10ng/mL). The biological activity dropped when the concentration was reduced to 1ng/mL and almost ceased to 0 when the concentration was increased to 100ng/mL.

It is not uncommon for chemokines to exhibit a biphasic response over a limited concentration range. In fact, SDF-1α itself has been reported to exhibit such a biphasic response (115, 116). A previous study has shown that over the concentration range of 0

to 1000nM, chemotactic activity of SDF-1α peaks at a concentration of 30nM. Its activity dropped when the concentration was increased or decreased and ceased to almost 0 when the concentration reached the upper limit of 1000nM (115). This result is consistent with our observation with commercial and WT-SDF-1α. In this study, SDF-1α concentrations tested were 1, 10, and 100ng/mL, which correspond to 0.1, 1, and 10nM, respectively. The highest concentration tested is still lower than the 30nM, concentration that induces the peaked SDF-1α activity. As a result, both commercial and WT-SDF-1α showed only positive correlation between its concentration and activity.

The biphasic response of SDF-1α can be attributed to its oligomeric state. SDF-1α has been previously reported to exist in monomer-dimer equilibriums (117). Monomeric SDF-1α is biologically active and able to induce chemotaxis, while SDF-1α in its dimeric form is biologically inactive (115, 118). For instance, researchers used engineered CXCL12 variants, which are wild-type $CXCL12_{WT}$, preferentially monomeric ($CXCL12_{H25R}$) and constitutively dimeric ($CXCL12_2$) chemokine to examine the migration of HCT 116 colorectal carcinoma cells and HT29 epithelial cells. The results have demonstrated that both $CXCL12_{WT}$ and $CXCL12_{H25R}$ were able to induce chemotaxis, yet $CXCL12_2$ failed to be bioactive (118).

From the collaborative observation on the biphasic response of SDF-1α and its reported opposing activities at different oligomeric states, we speculate that introducing an extra cysteine residue on the *C*-terminus of SDF-1α has the potential to make it more prone to dimer formation, and hence shifts the monomer-dimer equilibrium and results in a peaked chemotactic activity at a lower concentration. Cysteine is a biologically active residue; its thiol group can be easily oxidized to form a bond. Introducing an extra free cysteine to SDF-1α potentially increased the possibility of formation of undesired intermolecular bonds. Since the active site of SDF-1α is on the *N*-terminus of the protein, it is unlikely the intermolecular interaction would completely diminish its activity. However, it might be sufficient to change the conformation and folding of SDF-1α. Proteins that are not properly folded form aggregation and precipitation more easily (119), which is consistent with the observation that Cys-SDF-1α had a lower yield than WT-SDF-1α under the same condition.

There are other factors that could influence the monomer-dimer equilibrium. For instance, pH of the solution could majorly affect the oligomeric state of SDF-1α (117). It was previously reported that acidic pH would destabilize the dimeric structure and promote the monomeric state. In this study, the storage buffer of SDF-1α has a pH of 7.9, at which the SDF-1α is more prone to dimerize. The culture media used during chemotaxis assay has a physiological pH of 7.4. Although this is still basic, it is slightly more acidic than the storage buffer. Prior to chemotaxis assay, SDF-1αs in the storage buffer was diluted with culture media to reach the desired concentration. More concentrated SDF-1αs requires less dilution, so a more concentrated sample would have a more basic pH compared to less concentrated sample. The pH effect in combination with the extra free active cysteine might explain why the chemotactic activity of Cys-SDF-1α peaked at a shifted, lower concentration than previously reported.

In addition to *in vitro* chemotactic activities, the *in vivo* biological activity of engineered Cys-SDF-1α was investigated using a transgenic TIE-2-GFP mouse model. TIE-2 is an angiopoietin receptor that binds to required protein growth factors for angiogenesis. Results showed that at the concentration tested, which was 25 ng/mL, TIE-2 expression induced by commercial SDF-1α and Cys-SDF-1α did not differ appreciably.

There are many factors in this *in vivo* study that make the results not fully reliable and conclusive. First of all, the sample size is not adequate to draw a reliable conclusion. The study began with 3 mice. Each mouse was implanted with a whole set of experimental groups (plain control, commercial and Cys-SDF-1α at 25ng/mL). Unfortunately, the implanted hydrogel were very fragile, and the surgery sites were easily scratched by the mice. Consequently, during the two weeks of implantation, two out of three mice had damaged some of its implanted hydrogels in varying degrees. Mice have strong individual variation; therefore it is only accurate to compare groups harvested from the same mouse. As a result, only one hydrogel sample from each experimental group was imaged and compared. To draw a more convincing conclusion, the *in vivo* study should be repeated with a larger sample size. Second of all, the concentration of SDF-1α used in this study might be too low to detect a real difference. As stated earlier, the SDF-1α is very tiny in size, hence has a fast diffusion rate, which is further accelerated under an *in vivo* environment. As a result, the actual concentration of SDF-1α at the targeted sites is unknown; it is expected to be much lower than 25ng/mL. It is possible that the activities of commercial and cys-SDF-1α do not significantly differ at this low effective concentration. Due to the technical limitation in this study, 25ng/mL is the most concentrated hydrogel we were able to achieve. For future work, more optimization need to be done to increase protein yield of Cys-SDF-1α and the *in vivo* study should be repeated with more samples with higher concentrations.

In this study, we engineered a Cys-SDF-1α by introducing a cysteine residue to the *C*-terminus of the SDF-1α. Due to the limited timeframe and access to facilities, this project is only the first step in a promising development in this field. One major step is to improve the purification of the protein. Subsequently, more chemical analysis, such as NMR and X-ray crystallography should be performed on the purified Cys-SDF-1α. In addition, the biological activities of Cys-SDF-1α need to be further characterized. For instance, the chemotaxis assay was performed in this studying using Jurkat cells. In the future, chemotaxis study should be repeated with other CXCR4/7 positive cells such as endothelial or muscle cells.

Chapter 5: Concluding Remarks

The field of tissue engineering and regenerative medicine first emerged approximately three decades ago and has undergone rapid development ever since. With the goal of generating an artificial replacement for diseased or trauma-damaged native tissue or organs, tissue engineering and regenerative medicine is on the forefront of significantly improving a patient's health and welfare. Constructing a tissue organ that will function properly and efficiently *in vivo* requires comprehensive understanding of the complex biological system, including how native body reacts and responds to biomaterials and biochemical stimuli, individually or in combination. Improved information and knowledge on this ever-growing field will guide scientists in future studies to improve current technology or design better platforms for various medical applications.

Cardiovascular diseases not only majorly affect a patient's life quality; it is also an enormous socioeconomic burden. In an effort to advance the treatment of cardiovascular diseases, the primary focus of this dissertation is improving vascular regeneration from the perspective of biodegradable scaffolds and biochemical cues. We began the study by developing and optimizing a working small-diameter vascular graft. Based on the architectural integrity and extent of cell infiltration, we subsequently screened and selected a promising candidate whose *in vivo* performance was investigated. In addition, the effect of an angiogenesis-promoting chemokine in combination with the vascular grafts on vascular regeneration was studied. In particular, the endothelialization of the luminal surface of the vascular grafts and vascular wall remodeling were investigated. Lastly, we protein-engineered the previously employed angiogenesis-promoting chemokine in an attempt to broaden its biomedical application.

In Chapter 2, we focused on the optimization of vascular grafts. Having adequate cell infiltration into vascular grafts has always been a major challenge. On the one hand, an ideal biomaterial would be bioinert and trigger little to no inflammatory responses. On the other hand, however, a bioinert material would non-specifically downregulate biological responses, such as protein adsorption and cell attachment. In other words, while bioinert biomaterials recruit little detrimental inflammatory cells, they also reject many favorable and essential cells for tissue regeneration, such as endothelial and smooth muscle cells. In order to promote cell infiltration, the pore size of PLCL scaffolds was increased by modulating electrospinning parameters. Unfortunately, cell infiltration was only enhanced marginally. We then employed a fast-degrading polymer PDO, which has a more polar chemical structure than PLCL. We designed various single- and multi-layered vascular grafts and observed a weak adhesion between PLCL and PDO, potentially due to the difference in their polarity. We showed while electrospun PDO grafts have less structural integrity compared to PLCL grafts, using fast-degrading PDO drastically enhanced cell infiltration. This observation suggests that the unfavorable hydrophobicity of PLCL vascular grafts prevents cells from adhering despite its pore size. Among all the scaffold designs, we showed that PLCL/PDO blend vascular grafts provide the best balance between structural integrity and cell infiltration. In this chapter, we have demonstrated the methodology for developing a vascular graft that promotes

cell infiltration and allows us to investigate vascular regeneration in our subsequent *in vivo* studies. The advances achieved in this work improved our understanding of biomaterials and built a foundation for future development of an applicable vascular graft.

In Chapter 3, we investigated the effect of the cell-free PLCL/PDO blend vascular grafts developed in Chapter 2 and angiogenesis-promoting chemokine SDF-1α on vascular regeneration. In particular, the degree and extent of endothelialization and remodeling of the vascular wall were examined. We have demonstrated that partial endothelialization of the grafts took place as early as 2 weeks after implantation. The SDF-1α improved long-term patency presumably by recruiting and promoting proliferation of endothelial cells, which leads to a more complete anti-thrombogenic surface. Moreover, we have demonstrated that SDF-1α improved the vascular wall remodeling by recruiting smooth muscle cells. In addition to the favorable endothelial and smooth muscle cells, we have observed recruitment of inflammatory cells as well. However, we did not observe calcification, which is a destructive vascular surgery complication induced by inflammatory responses. A comparison between this investigation and a similar recent study showed that when the vascular grafts are fabricated with different biomaterials, the degree and extent of vascular regeneration promoted by SDF-1α also varies. This observation suggests that biomaterials and biomolecules have a collaborative "effect." More studies are recommended to explore the optimal combination that will work in synergy. The investigation detailed in Chapter 3 has demonstrated that the host possesses endogenous regeneration potential and is capable of vascular regenerating if we are able to engineer optimized vascular grafts to harness this potential.

In Chapter 4, we transitioned from a biomaterial perspective to a biochemical focus. In an effort to broaden its biological applications, we protein engineered SDF-1α, the angiogenesis-promoting chemokine we employed in Chapter 3. In this study, we introduced an amino acid cysteine to the *C*-terminus of SDF-1α. The cysteine modification allows SDF-1α to be subsequently conjugated using many well established chemistry reactions without disturbing its active *N*-terminus. We expressed, isolated, refolded, and purified the cysteine-modified SDF-1α and investigated its *in vitro* chemotactic activity. We have shown that the cysteine-modified SDF-1α exhibits a biphasic response over the concentration range tested in this study. Although it has been reported that wild-type SDF-1α does exhibit a biphasic response, the peak concentration is much lower for cysteine-modified SDF-1α. We hypothesized that the extra cysteine residue results in a SDF-1α more prone to dimer formation, which diminishes the bioactivity of SDF-1α. Future studies are required to analyze the structure of cysteine-modified SDF-1α and optimize the purification process. The results reported herein have laid a foundation for future designs of medicine for various therapeutic applications such as tissue ischemia treatment.

In work detailed in this dissertation, we investigated biomaterial and biochemical approaches in an attempt to enhance vascular regeneration by improving cell infiltration and recruitment of essential cells, while maintaining optimal mechanical properties of

the vascular grafts. The information gleaned from this study has contributed to our understanding of vascular regeneration by learning how native tissue interacts with biodegradable vascular grafts and angiogenesis-promoting biomolecules. The findings from this dissertation provide much needed insight into the field of vascular grafts and provide a path for future studies to tune and improve vascular grafts technology on both an architectural and compositional level, as well as to develop angiogenetic medicine. These, in turn, will lead to the acceleration of the functional vascularization and may yield benefit for therapeutic applications.

References

1. Zhang B, Pu WT. Notching up vascular regeneration. Cell research. 2014;24(7):777-8. doi: 10.1038/cr.2014.68. PubMed PMID: 24853955; PubMed Central PMCID: PMC4085764.

2. Levenberg S, Langer R. Advances in tissue engineering. Current topics in developmental biology. 2004;61:113-34. doi: 10.1016/S0070-2153(04)61005-2. PubMed PMID: 15350399.

3. Vacanti CA. History of tissue engineering and a glimpse into its future. Tissue engineering. 2006;12(5):1137-42. doi: 10.1089/ten.2006.12.1137. PubMed PMID: 16771629.

4. Mikos AG, Herring SW, Ochareon P, Elisseeff J, Lu HH, Kandel R, et al. Engineering complex tissues. Tissue engineering. 2006;12(12):3307-39. doi: 10.1089/ten.2006.12.3307. PubMed PMID: 17518671; PubMed Central PMCID: PMC2821210.

5. Nerem RM, Sambanis A. Tissue engineering: from biology to biological substitutes. Tissue engineering. 1995;1(1):3-13. doi: 10.1089/ten.1995.1.3. PubMed PMID: 19877911.

6. Deaths: Preliminary Data for 2012. In: Prevention CfDCa, editor. 2012.

7. Atlas of Heart Disease and Stroke. In: Organization WH, editor. 2004.

8. Li S, Sengupta D, Chien S. Vascular tissue engineering: from in vitro to in situ. Wiley interdisciplinary reviews Systems biology and medicine. 2014;6(1):61-76. doi: 10.1002/wsbm.1246. PubMed PMID: 24151038.

9. Roll S, Muller-Nordhorn J, Keil T, Scholz H, Eidt D, Greiner W, et al. Dacron vs. PTFE as bypass materials in peripheral vascular surgery--systematic review and meta-analysis. BMC surgery. 2008;8:22. doi: 10.1186/1471-2482-8-22. PubMed PMID: 19099583; PubMed Central PMCID: PMC2645354.

10. Sayers RD, Raptis S, Berce M, Miller JH. Long-term results of femorotibial bypass with vein or polytetrafluoroethylene. The British journal of surgery. 1998;85(7):934-8. doi: 10.1046/j.1365-2168.1998.00765.x. PubMed PMID: 9692567.

11. Cleary MA, Geiger E, Grady C, Best C, Naito Y, Breuer C. Vascular tissue engineering: the next generation. Trends in molecular medicine. 2012;18(7):394-404. doi: 10.1016/j.molmed.2012.04.013. PubMed PMID: 22695236.

12. Zdrahala RJ. Small caliber vascular grafts. Part I: state of the art. Journal of biomaterials applications. 1996;10(4):309-29. PubMed PMID: 8859403.

13. Zdrahala RJ. Small caliber vascular grafts. Part II: Polyurethanes revisited. Journal of biomaterials applications. 1996;11(1):37-61. PubMed PMID: 8872599.

14. Kaushal S, Amiel GE, Guleserian KJ, Shapira OM, Perry T, Sutherland FW, et al. Functional small-diameter neovessels created using endothelial progenitor cells expanded ex vivo. Nature medicine. 2001;7(9):1035-40. doi: 10.1038/nm0901-1035. PubMed PMID: 11533707; PubMed Central PMCID: PMC2818999.

15. Gui L, Muto A, Chan SA, Breuer CK, Niklason LE. Development of decellularized human umbilical arteries as small-diameter vascular grafts. Tissue engineering Part A. 2009;15(9):2665-76. doi: 10.1089/ten.TEA.2008.0526. PubMed PMID: 19207043; PubMed Central PMCID: PMC2735599.

16. Dahl SL, Kypson AP, Lawson JH, Blum JL, Strader JT, Li Y, et al. Readily available tissue-engineered vascular grafts. Science translational medicine. 2011;3(68):68ra9. doi: 10.1126/scitranslmed.3001426. PubMed PMID: 21289273.

17. Hashi CK, Zhu Y, Yang GY, Young WL, Hsiao BS, Wang K, et al. Antithrombogenic property of bone marrow mesenchymal stem cells in nanofibrous vascular grafts. Proceedings of the National Academy of Sciences of the United States of America. 2007;104(29):11915-20. doi: 10.1073/pnas.0704581104. PubMed PMID: 17615237; PubMed Central PMCID: PMC1924591.

18. Yu J, Wang A, Tang Z, Henry J, Li-Ping Lee B, Zhu Y, et al. The effect of stromal cell-derived factor-1alpha/heparin coating of biodegradable vascular grafts on the recruitment of both endothelial and smooth muscle progenitor cells for accelerated regeneration. Biomaterials. 2012;33(32):8062-74. doi: 10.1016/j.biomaterials.2012.07.042. PubMed PMID: 22884813; PubMed Central PMCID: PMC3488434.

19. Liang D, Hsiao BS, Chu B. Functional electrospun nanofibrous scaffolds for biomedical applications. Advanced drug delivery reviews. 2007;59(14):1392-412. doi: 10.1016/j.addr.2007.04.021. PubMed PMID: 17884240; PubMed Central PMCID: PMC2693708.

20. Anielle An-Chi Tsou SL. Engineering Microenvironments to Control Stem Cell Functions. In: Uma Lakshmipathy JDC, Bhaskar Thyagarajan, editor. Emerging Technology Platforms for Stem Cells: John Wiley & Sons, Inc.; 2009. p. 311-26.

21. Barnes CP, Sell SA, Boland ED, Simpson DG, Bowlin GL. Nanofiber technology: designing the next generation of tissue engineering scaffolds. Advanced drug delivery reviews. 2007;59(14):1413-33. doi: 10.1016/j.addr.2007.04.022. PubMed PMID: 17916396.

22. Wang HB, Mullins ME, Cregg JM, McCarthy CW, Gilbert RJ. Varying the diameter of aligned electrospun fibers alters neurite outgrowth and Schwann cell

migration. Acta biomaterialia. 2010;6(8):2970-8. doi: 10.1016/j.actbio.2010.02.020. PubMed PMID: 20167292.

23. Bhardwaj N, Kundu SC. Electrospinning: a fascinating fiber fabrication technique. Biotechnology advances. 2010;28(3):325-47. doi: 10.1016/j.biotechadv.2010.01.004. PubMed PMID: 20100560.

24. Seeram Ramakrishna KF, Wee-Eong Teo, Teik-Cheng Lim, Zuwei Ma,. An Introduction to Electrospinning and Nanofibers. Singapore: World Scientific; 2005.

25. Zheng-Ming Huang Y-ZZ, M. Kotaki, S. Ramakrishna,. A review on polymer nanofibers by electrospinning and their applications in nanocomposites. Composites Science and Technology. 2003;63(15):2223-53.

26. Piskin E, Bolgen N, Egri S, Isoglu IA. Electrospun matrices made of poly(alpha-hydroxy acids) for medical use. Nanomedicine. 2007;2(4):441-57. doi: 10.2217/17435889.2.4.441. PubMed PMID: 17716131.

27. V Hasirci PY, T Endogan, G Eke, N Hasirci, . Polymer Fundamentals: Polymer Synthesis. In: Paul Ducheyne KEH, Dietmar W. Hutmacher, David W. Grainger, C. James Kirkpatrick, editor. Comprehensive Biomaterials: Elsevier Ltd.; 2011. p. 349-71.

28. Hayashi T. Biodegradable polymers for biomedical uses. Progress in Polymer Science. 1994;19(4):663-702.

29. Jeong SI, Kim BS, Lee YM, Ihn KJ, Kim SH, Kim YH. Morphology of elastic poly(L-lactide-co-epsilon-caprolactone) copolymers and in vitro and in vivo degradation behavior of their scaffolds. Biomacromolecules. 2004;5(4):1303-9. doi: 10.1021/bm049921i. PubMed PMID: 15244444.

30. Kim SH, Kwon JH, Chung MS, Chung E, Jung Y, Kim SH, et al. Fabrication of a new tubular fibrous PLCL scaffold for vascular tissue engineering. Journal of biomaterials science Polymer edition. 2006;17(12):1359-74. PubMed PMID: 17260508.

31. Fu W, Liu Z, Feng B, Hu R, He X, Wang H, et al. Electrospun gelatin/PCL and collagen/PLCL scaffolds for vascular tissue engineering. International journal of nanomedicine. 2014;9:2335-44. doi: 10.2147/IJN.S61375. PubMed PMID: 24872696; PubMed Central PMCID: PMC4026554.

32. Shalaby SW JR. Synthetic absorbable polyesters. In: SW S, editor. Biomedical polymers Designed to degrade systems New York: Hanser; 1994. p. 1-34.

33. Ray JA, Doddi N, Regula D, Williams JA, Melveger A. Polydioxanone (PDS), a novel monofilament synthetic absorbable suture. Surgery, gynecology & obstetrics. 1981;153(4):497-507. PubMed PMID: 6792722.

34. Middleton JC, Tipton AJ. Synthetic biodegradable polymers as orthopedic devices. Biomaterials. 2000;21(23):2335-46. PubMed PMID: 11055281.

35. Boland ED, Coleman BD, Barnes CP, Simpson DG, Wnek GE, Bowlin GL. Electrospinning polydioxanone for biomedical applications. Acta biomaterialia. 2005;1(1):115-23. doi: 10.1016/j.actbio.2004.09.003. PubMed PMID: 16701785.

36. Dorigo W, Pulli R, Piffaretti G, Castelli P, Griselli F, Dorrucci V, et al. Results from an Italian multicentric registry comparing heparin-bonded ePTFE graft and autologous saphenous vein in below-knee femoro-popliteal bypasses. The Journal of cardiovascular surgery. 2012;53(2):187-94. PubMed PMID: 22456641.

37. Roh JD, Sawh-Martinez R, Brennan MP, Jay SM, Devine L, Rao DA, et al. Tissue-engineered vascular grafts transform into mature blood vessels via an inflammation-mediated process of vascular remodeling. Proceedings of the National Academy of Sciences of the United States of America. 2010;107(10):4669-74. doi: 10.1073/pnas.0911465107. PubMed PMID: 20207947; PubMed Central PMCID: PMC2842056.

38. He W, Nieponice A, Soletti L, Hong Y, Gharaibeh B, Crisan M, et al. Pericyte-based human tissue engineered vascular grafts. Biomaterials. 2010;31(32):8235-44. doi: 10.1016/j.biomaterials.2010.07.034. PubMed PMID: 20684982; PubMed Central PMCID: PMC3178347.

39. Neff LP, Tillman BW, Yazdani SK, Machingal MA, Yoo JJ, Soker S, et al. Vascular smooth muscle enhances functionality of tissue-engineered blood vessels in vivo. Journal of vascular surgery. 2011;53(2):426-34. doi: 10.1016/j.jvs.2010.07.054. PubMed PMID: 20934837.

40. Zhu C, Ying D, Mi J, Li L, Zeng W, Hou C, et al. Development of anti-atherosclerotic tissue-engineered blood vessel by A20-regulated endothelial progenitor cells seeding decellularized vascular matrix. Biomaterials. 2008;29(17):2628-36. doi: 10.1016/j.biomaterials.2008.03.005. PubMed PMID: 18377984.

41. Kim TG, Chung HJ, Park TG. Macroporous and nanofibrous hyaluronic acid/collagen hybrid scaffold fabricated by concurrent electrospinning and deposition/leaching of salt particles. Acta biomaterialia. 2008;4(6):1611-9. doi: 10.1016/j.actbio.2008.06.008. PubMed PMID: 18640884.

42. Homa Homayoni SAHR, Masoumeh Valizadeh. Electrospinning of chitosan nanofibers: Processing optimization. Carbohydrate polymers. 2009;77(3):656-61.

43. Mohammad Chowdhury GS. Effect of Experimental Parameters on the Morphology of Electrospun Nylon 6 fibres. International Journal of Basic & Applied Sciences IJBAS-IJENS. 2010;10(06):70-8.

44. Wu W, Allen RA, Wang Y. Fast-degrading elastomer enables rapid remodeling of a cell-free synthetic graft into a neoartery. Nature medicine. 2012;18(7):1148-53. doi: 10.1038/nm.2821. PubMed PMID: 22729285; PubMed Central PMCID: PMC3438366.

45. Jeffries EM, Allen RA, Gao J, Pesce M, Wang Y. Highly elastic and suturable electrospun poly(glycerol sebacate) fibrous scaffolds. Acta biomaterialia. 2015;18:30-9. doi: 10.1016/j.actbio.2015.02.005. PubMed PMID: 25686558; PubMed Central PMCID: PMC4395539.

46. Ishii D, Ying TH, Mahara A, Murakami S, Yamaoka T, Lee WK, et al. In vivo tissue response and degradation behavior of PLLA and stereocomplexed PLA nanofibers. Biomacromolecules. 2009;10(2):237-42. doi: 10.1021/bm8009363. PubMed PMID: 19117403.

47. Telemeco TA, Ayres C, Bowlin GL, Wnek GE, Boland ED, Cohen N, et al. Regulation of cellular infiltration into tissue engineering scaffolds composed of submicron diameter fibrils produced by electrospinning. Acta biomaterialia. 2005;1(4):377-85. doi: 10.1016/j.actbio.2005.04.006. PubMed PMID: 16701819.

48. Pan JF, Liu NH, Shu LY, Sun H. Application of avidin-biotin technology to improve cell adhesion on nanofibrous matrices. Journal of nanobiotechnology. 2015;13:37. doi: 10.1186/s12951-015-0096-2. PubMed PMID: 25980573; PubMed Central PMCID: PMC4461904.

49. College O. Anatomy & Physiology, 1st edition: OpenStax College; 2013.

50. Vinay Kumar AKA, Jon C. Aster. Robbins Basic Pathology, 9th edition: Saunder; 2012.

51. Arshady R. Polymeric biomaterials: chemistry, concepts, criteria. In: R A, editor. Introduction to polymeric biomaterials: the polymeric biomaterials series: Citus Books; 2003. p. 1-62.

52. Schoen FJ AJ. Host response to biomaterials and their evaluation. In: Ratner BD SF, Lemons JE, editor. Biomaterials Science: an Introduction to Materials in Medicine, 2nd edition. San Diego: Elsevier; 2004. p. 293-6.

53. B.A. Ratner TAH. Some background concepts. In: Buddy D. Ratner FJS, Jack E. Lemons editor. Biomaterials science: an introduction to materials in medicine: Elsevier; 2004. p. 237.

54. Ratner BD, Bryant SJ. Biomaterials: where we have been and where we are going. Annual review of biomedical engineering. 2004;6:41-75. doi: 10.1146/annurev.bioeng.6.040803.140027. PubMed PMID: 15255762.

55. Anderson JM. Inflammatory response to implants. ASAIO transactions / American Society for Artificial Internal Organs. 1988;34(2):101-7. PubMed PMID: 3285869.

56. Jutila MA. Leukocyte traffic to sites of inflammation. APMIS : acta pathologica, microbiologica, et immunologica Scandinavica. 1992;100(3):191-201. PubMed PMID: 1373285.

57. Pober JS, Cotran RS. The role of endothelial cells in inflammation. Transplantation. 1990;50(4):537-44. PubMed PMID: 2219269.

58. Williams GT, Williams WJ. Granulomatous inflammation--a review. Journal of clinical pathology. 1983;36(7):723-33. PubMed PMID: 6345591; PubMed Central PMCID: PMC498378.

59. Wahl SM, Wong H, McCartney-Francis N. Role of growth factors in inflammation and repair. Journal of cellular biochemistry. 1989;40(2):193-9. doi: 10.1002/jcb.240400208. PubMed PMID: 2670976.

60. Johnston RB, Jr. Current concepts: immunology. Monocytes and macrophages. The New England journal of medicine. 1988;318(12):747-52. doi: 10.1056/NEJM198803243181205. PubMed PMID: 3279314.

61. Kovacs EJ. Fibrogenic cytokines: the role of immune mediators in the development of scar tissue. Immunology today. 1991;12(1):17-23. doi: 10.1016/0167-5699(91)90107-5. PubMed PMID: 2015044.

62. Pierce GF, Mustoe TA, Altrock BW, Deuel TF, Thomason A. Role of platelet-derived growth factor in wound healing. Journal of cellular biochemistry. 1991;45(4):319-26. doi: 10.1002/jcb.240450403. PubMed PMID: 2045423.

63. Labat-Robert J, Bihari-Varga M, Robert L. Extracellular matrix. FEBS letters. 1990;268(2):386-93. PubMed PMID: 2166694.

64. Anderson JM, Rodriguez A, Chang DT. Foreign body reaction to biomaterials. Seminars in immunology. 2008;20(2):86-100. doi: 10.1016/j.smim.2007.11.004. PubMed PMID: 18162407; PubMed Central PMCID: PMC2327202.

65. Kenneth Murphy PT, Mark Walport. Janeway's Immunobiology, 7th edition: Garland Science; 2007.

66. Mantovani A, Sica A, Sozzani S, Allavena P, Vecchi A, Locati M. The chemokine system in diverse forms of macrophage activation and polarization. Trends in immunology. 2004;25(12):677-86. doi: 10.1016/j.it.2004.09.015. PubMed PMID: 15530839.

67. Stout RD, Jiang C, Matta B, Tietzel I, Watkins SK, Suttles J. Macrophages sequentially change their functional phenotype in response to changes in microenvironmental influences. Journal of immunology. 2005;175(1):342-9. PubMed PMID: 15972667.

68. Badylak SF, Valentin JE, Ravindra AK, McCabe GP, Stewart-Akers AM. Macrophage phenotype as a determinant of biologic scaffold remodeling. Tissue engineering Part A. 2008;14(11):1835-42. doi: 10.1089/ten.tea.2007.0264. PubMed PMID: 18950271.

69. Brown BN, Londono R, Tottey S, Zhang L, Kukla KA, Wolf MT, et al. Macrophage phenotype as a predictor of constructive remodeling following the implantation of biologically derived surgical mesh materials. Acta biomaterialia. 2012;8(3):978-87. doi: 10.1016/j.actbio.2011.11.031. PubMed PMID: 22166681; PubMed Central PMCID: PMC4325370.

70. Garg K, Pullen NA, Oskeritzian CA, Ryan JJ, Bowlin GL. Macrophage functional polarization (M1/M2) in response to varying fiber and pore dimensions of electrospun scaffolds. Biomaterials. 2013;34(18):4439-51. doi: 10.1016/j.biomaterials.2013.02.065. PubMed PMID: 23515178; PubMed Central PMCID: PMC3623371.

71. de Valence S, Tille JC, Mugnai D, Mrowczynski W, Gurny R, Moller M, et al. Long term performance of polycaprolactone vascular grafts in a rat abdominal aorta replacement model. Biomaterials. 2012;33(1):38-47. doi: 10.1016/j.biomaterials.2011.09.024. PubMed PMID: 21940044.

72. Amara A, Lorthioir O, Valenzuela A, Magerus A, Thelen M, Montes M, et al. Stromal cell-derived factor-1alpha associates with heparan sulfates through the first beta-strand of the chemokine. The Journal of biological chemistry. 1999;274(34):23916-25. PubMed PMID: 10446158.

73. Murphy JW, Cho Y, Sachpatzidis A, Fan C, Hodsdon ME, Lolis E. Structural and functional basis of CXCL12 (stromal cell-derived factor-1 alpha) binding to heparin. The Journal of biological chemistry. 2007;282(13):10018-27. doi: 10.1074/jbc.M608796200. PubMed PMID: 17264079; PubMed Central PMCID: PMC3684283.

74. Sadir R, Baleux F, Grosdidier A, Imberty A, Lortat-Jacob H. Characterization of the stromal cell-derived factor-1alpha-heparin complex. The Journal of biological chemistry. 2001;276(11):8288-96. doi: 10.1074/jbc.M008110200. PubMed PMID: 11087743.

75. Sadir R, Imberty A, Baleux F, Lortat-Jacob H. Heparan sulfate/heparin oligosaccharides protect stromal cell-derived factor-1 (SDF-1)/CXCL12 against proteolysis induced by CD26/dipeptidyl peptidase IV. The Journal of biological chemistry. 2004;279(42):43854-60. doi: 10.1074/jbc.M405392200. PubMed PMID: 15292258.

76. Yamaguchi J, Kusano KF, Masuo O, Kawamoto A, Silver M, Murasawa S, et al. Stromal cell-derived factor-1 effects on ex vivo expanded endothelial progenitor cell recruitment for ischemic neovascularization. Circulation. 2003;107(9):1322-8. PubMed PMID: 12628955.

77. Salvucci O, Yao L, Villalba S, Sajewicz A, Pittaluga S, Tosato G. Regulation of endothelial cell branching morphogenesis by endogenous chemokine stromal-derived factor-1. Blood. 2002;99(8):2703-11. PubMed PMID: 11929756.

78. Zilla P, Bezuidenhout D, Human P. Prosthetic vascular grafts: wrong models, wrong questions and no healing. Biomaterials. 2007;28(34):5009-27. doi: 10.1016/j.biomaterials.2007.07.017. PubMed PMID: 17688939.

79. Bull DA, Hunter GC, Holubec H, Aguirre ML, Rappaport WD, Putnam CW. Cellular origin and rate of endothelial cell coverage of PTFE grafts. The Journal of surgical research. 1995;58(1):58-68. doi: 10.1006/jsre.1995.1010. PubMed PMID: 7830407.

80. Aikawa E, Nahrendorf M, Figueiredo JL, Swirski FK, Shtatland T, Kohler RH, et al. Osteogenesis associates with inflammation in early-stage atherosclerosis evaluated by molecular imaging in vivo. Circulation. 2007;116(24):2841-50. doi: 10.1161/CIRCULATIONAHA.107.732867. PubMed PMID: 18040026.

81. Aikawa E, Aikawa M, Libby P, Figueiredo JL, Rusanescu G, Iwamoto Y, et al. Arterial and aortic valve calcification abolished by elastolytic cathepsin S deficiency in chronic renal disease. Circulation. 2009;119(13):1785-94. doi: 10.1161/CIRCULATIONAHA.108.827972. PubMed PMID: 19307473; PubMed Central PMCID: PMC2717745.

82. Tintut Y, Patel J, Parhami F, Demer LL. Tumor necrosis factor-alpha promotes in vitro calcification of vascular cells via the cAMP pathway. Circulation. 2000;102(21):2636-42. PubMed PMID: 11085968.

83. New SE, Aikawa E. Molecular imaging insights into early inflammatory stages of arterial and aortic valve calcification. Circulation research. 2011;108(11):1381-91. doi: 10.1161/CIRCRESAHA.110.234146. PubMed PMID: 21617135; PubMed Central PMCID: PMC3139950.

84. Mehta RI, Mukherjee AK, Patterson TD, Fishbein MC. Pathology of explanted polytetrafluoroethylene vascular grafts. Cardiovascular pathology : the official journal of the Society for Cardiovascular Pathology. 2011;20(4):213-21. doi: 10.1016/j.carpath.2010.06.005. PubMed PMID: 20619685.

85. Fernandez EJ, Lolis E. Structure, function, and inhibition of chemokines. Annual review of pharmacology and toxicology. 2002;42:469-99. doi: 10.1146/annurev.pharmtox.42.091901.115838. PubMed PMID: 11807180.

86. Lapidot T, Petit I. Current understanding of stem cell mobilization: the roles of chemokines, proteolytic enzymes, adhesion molecules, cytokines, and stromal cells. Experimental hematology. 2002;30(9):973-81. PubMed PMID: 12225788.

87. Horuk R. Chemokine receptors. Cytokine & growth factor reviews. 2001;12(4):313-35. PubMed PMID: 11544102.

88. Bagri A, Gurney T, He X, Zou YR, Littman DR, Tessier-Lavigne M, et al. The chemokine SDF1 regulates migration of dentate granule cells. Development. 2002;129(18):4249-60. PubMed PMID: 12183377.

89. Strieter RM, Burdick MD, Mestas J, Gomperts B, Keane MP, Belperio JA. Cancer CXC chemokine networks and tumour angiogenesis. European journal of cancer. 2006;42(6):768-78. doi: 10.1016/j.ejca.2006.01.006. PubMed PMID: 16510280.

90. Schier AF. Chemokine signaling: rules of attraction. Current biology : CB. 2003;13(5):R192-4. PubMed PMID: 12620211.

91. Broxmeyer HE, Cooper S, Kohli L, Hangoc G, Lee Y, Mantel C, et al. Transgenic expression of stromal cell-derived factor-1/CXC chemokine ligand 12 enhances myeloid progenitor cell survival/antiapoptosis in vitro in response to growth factor withdrawal and enhances myelopoiesis in vivo. Journal of immunology. 2003;170(1):421-9. PubMed PMID: 12496427.

92. Nagasawa T, Hirota S, Tachibana K, Takakura N, Nishikawa S, Kitamura Y, et al. Defects of B-cell lymphopoiesis and bone-marrow myelopoiesis in mice lacking the CXC chemokine PBSF/SDF-1. Nature. 1996;382(6592):635-8. doi: 10.1038/382635a0. PubMed PMID: 8757135.

93. Ma Q, Jones D, Springer TA. The chemokine receptor CXCR4 is required for the retention of B lineage and granulocytic precursors within the bone marrow microenvironment. Immunity. 1999;10(4):463-71. PubMed PMID: 10229189.

94. Lu W, Gersting JA, Maheshwari A, Christensen RD, Calhoun DA. Developmental expression of chemokine receptor genes in the human fetus. Early human development. 2005;81(6):489-96. doi: 10.1016/j.earlhumdev.2004.10.022. PubMed PMID: 15935926.

95. Balabanian K, Lagane B, Infantino S, Chow KY, Harriague J, Moepps B, et al. The chemokine SDF-1/CXCL12 binds to and signals through the orphan receptor RDC1 in T lymphocytes. The Journal of biological chemistry. 2005;280(42):35760-6. doi: 10.1074/jbc.M508234200. PubMed PMID: 16107333.

96. Shirozu M, Nakano T, Inazawa J, Tashiro K, Tada H, Shinohara T, et al. Structure and chromosomal localization of the human stromal cell-derived factor 1 (SDF1) gene. Genomics. 1995;28(3):495-500. doi: 10.1006/geno.1995.1180. PubMed PMID: 7490086.

97. Janowski M. Functional diversity of SDF-1 splicing variants. Cell adhesion & migration. 2009;3(3):243-9. PubMed PMID: 19287206; PubMed Central PMCID: PMC2712802.

98. Murdoch C, Monk PN, Finn A. Cxc chemokine receptor expression on human endothelial cells. Cytokine. 1999;11(9):704-12. doi: 10.1006/cyto.1998.0465. PubMed PMID: 10479407.

99. Kucia M, Ratajczak J, Reca R, Janowska-Wieczorek A, Ratajczak MZ. Tissue-specific muscle, neural and liver stem/progenitor cells reside in the bone marrow, respond to an SDF-1 gradient and are mobilized into peripheral blood during stress and tissue injury. Blood cells, molecules & diseases. 2004;32(1):52-7. PubMed PMID: 14757413.

100. Ratajczak MZ, Majka M, Kucia M, Drukala J, Pietrzkowski Z, Peiper S, et al. Expression of functional CXCR4 by muscle satellite cells and secretion of SDF-1 by muscle-derived fibroblasts is associated with the presence of both muscle progenitors in bone marrow and hematopoietic stem/progenitor cells in muscles. Stem cells. 2003;21(3):363-71. doi: 10.1634/stemcells.21-3-363. PubMed PMID: 12743331.

101. Ratajczak MZ, Zuba-Surma E, Kucia M, Reca R, Wojakowski W, Ratajczak J. The pleiotropic effects of the SDF-1-CXCR4 axis in organogenesis, regeneration and tumorigenesis. Leukemia. 2006;20(11):1915-24. doi: 10.1038/sj.leu.2404357. PubMed PMID: 16900209.

102. Tilling L, Chowienczyk P, Clapp B. Progenitors in motion: mechanisms of mobilization of endothelial progenitor cells. British journal of clinical pharmacology. 2009;68(4):484-92. doi: 10.1111/j.1365-2125.2009.03486.x. PubMed PMID: 19843051; PubMed Central PMCID: PMC2780273.

103. Carrico IS. Chemoselective modification of proteins: hitting the target. Chemical Society reviews. 2008;37(7):1423-31. doi: 10.1039/b703364h. PubMed PMID: 18568168.

104. Gamblin DP, van Kasteren SI, Chalker JM, Davis BG. Chemical approaches to mapping the function of post-translational modifications. The FEBS journal. 2008;275(9):1949-59. doi: 10.1111/j.1742-4658.2008.06347.x. PubMed PMID: 18384382.

105. Foley TL, Burkart MD. Site-specific protein modification: advances and applications. Current opinion in chemical biology. 2007;11(1):12-9. doi: 10.1016/j.cbpa.2006.11.036. PubMed PMID: 17189712.

106. Qi D, Tann CM, Haring D, Distefano MD. Generation of new enzymes via covalent modification of existing proteins. Chemical reviews. 2001;101(10):3081-111. PubMed PMID: 11710063.

107. Hermanson GT. Bioconjugate Techniques, 3rd edition: Academic Press, Inc.; 2013.

108. Fodje MN, Al-Karadaghi S. Occurrence, conformational features and amino acid propensities for the pi-helix. Protein engineering. 2002;15(5):353-8. PubMed PMID: 12034854.

109. Stephanopoulos N, Francis MB. Choosing an effective protein bioconjugation strategy. Nature chemical biology. 2011;7(12):876-84. doi: 10.1038/nchembio.720. PubMed PMID: 22086289.

110. Crankshaw MW, Grant GA. Modification of cysteine. Current protocols in protein science / editorial board, John E Coligan [et al]. 2001;Chapter 15:Unit15 1. doi: 10.1002/0471140864.ps1501s03. PubMed PMID: 18429125.

111. Bleul CC, Fuhlbrigge RC, Casasnovas JM, Aiuti A, Springer TA. A highly efficacious lymphocyte chemoattractant, stromal cell-derived factor 1 (SDF-1). The Journal of experimental medicine. 1996;184(3):1101-9. PubMed PMID: 9064327; PubMed Central PMCID: PMC2192798.

112. Taylor S, Folkman J. Protamine is an inhibitor of angiogenesis. Nature. 1982;297(5864):307-12. PubMed PMID: 6176876.

113. Nissen NN, Shankar R, Gamelli RL, Singh A, DiPietro LA. Heparin and heparan sulphate protect basic fibroblast growth factor from non-enzymic glycosylation. The Biochemical journal. 1999;338 (Pt 3):637-42. PubMed PMID: 10051433; PubMed Central PMCID: PMC1220097.

114. Segers VF, Revin V, Wu W, Qiu H, Yan Z, Lee RT, et al. Protease-resistant stromal cell-derived factor-1 for the treatment of experimental peripheral artery disease. Circulation. 2011;123(12):1306-15. doi: 10.1161/CIRCULATIONAHA.110.991786. PubMed PMID: 21403096.

115. Veldkamp CT, Seibert C, Peterson FC, De la Cruz NB, Haugner JC, 3rd, Basnet H, et al. Structural basis of CXCR4 sulfotyrosine recognition by the chemokine SDF-1/CXCL12. Science signaling. 2008;1(37):ra4. doi: 10.1126/scisignal.1160755. PubMed PMID: 18799424; PubMed Central PMCID: PMC2692298.

116. Smith JM, Johanesen PA, Wendt MK, Binion DG, Dwinell MB. CXCL12 activation of CXCR4 regulates mucosal host defense through stimulation of epithelial cell migration and promotion of intestinal barrier integrity. American journal of physiology Gastrointestinal and liver physiology. 2005;288(2):G316-26. doi: 10.1152/ajpgi.00208.2004. PubMed PMID: 15358596.

117. Veldkamp CT, Peterson FC, Pelzek AJ, Volkman BF. The monomer-dimer equilibrium of stromal cell-derived factor-1 (CXCL 12) is altered by pH, phosphate,

sulfate, and heparin. Protein science : a publication of the Protein Society. 2005;14(4):1071-81. doi: 10.1110/ps.041219505. PubMed PMID: 15741341; PubMed Central PMCID: PMC2253449.

118. Drury LJ, Ziarek JJ, Gravel S, Veldkamp CT, Takekoshi T, Hwang ST, et al. Monomeric and dimeric CXCL12 inhibit metastasis through distinct CXCR4 interactions and signaling pathways. Proceedings of the National Academy of Sciences of the United States of America. 2011;108(43):17655-60. doi: 10.1073/pnas.1101133108. PubMed PMID: 21990345; PubMed Central PMCID: PMC3203819.

119. Maulik V. Trivedi JSL, and Teruna J. Siahaan. The role of thiols and disulfides in protein chemical and physical stability. Curr Protein Pept Sci. 2009;10(6):614-25.